

Journal of Geophysical Research: Solid Earth**RESEARCH ARTICLE**

10.1002/2017JB014106

Key Points:

- Crustal k in crystalline rock to 2000 mbgs decreases with $\log(k) = -1.5 \times \log(z) - 16.3$ as inferred from a database of 30,000 in situ k -estimations
- Depth, current seismotectonic activity, and tectonogeological history are the most important geological factors controlling k distribution
- New regression models allow to predict depth-dependent site scale permeability distribution

Supporting Information:

- Supporting Information S1

Correspondence to:

P. Achtziger-Zupančič,
peter.achtziger@erdw.ethz.ch

Citation:

Achtziger-Zupančič, P., S. Loew, and G. Mariéthoz (2017), A new global database to improve predictions of permeability distribution in crystalline rocks at site scale, *J. Geophys. Res. Solid Earth*, 122, 3513–3539, doi:10.1002/2017JB014106.

Received 20 FEB 2017

Accepted 16 APR 2017

Accepted article online 20 APR 2017

Published online 21 MAY 2017

A new global database to improve predictions of permeability distribution in crystalline rocks at site scale

P. Achtziger-Zupančič¹ , S. Loew¹ , and G. Mariéthoz²

¹Geologic Institute, ETH Zürich, Zürich, Switzerland, ²Institute of Earth Surface Dynamics, University of Lausanne, Lausanne, Switzerland

Abstract A comprehensive worldwide permeability data set has been compiled consisting of 29,000 in situ permeabilities from 221 publications and reports and delineating the permeability distribution in crystalline rocks into depths of 2000 meters below ground surface (mbgs). We analyze the influence of technical factors (measurement method, scale effects, preferential sampling, and hydraulic anisotropy) and geological factors (lithology, current stress regime, current seismotectonic activity, and long-term tectonogeological history) on the permeability distribution with depth, by using regression analysis and k -means clustering. The influence of preferential sampling and hydraulic anisotropy are negligible. A scale dependency is observed based on calculated rock test volumes equaling 0.6 orders of magnitude of permeability change per order of magnitude of rock volume tested. Based on the entire data set, permeability decreases as $\log(k) = -1.5 \times \log(z) - 16.3$ with permeability k (m^2) and positively increasing depth z (km), and depth is the main factor driving the permeability distribution. The permeability variance is about 2 orders of magnitude at all depths, presumably representing permeability variations around brittle fault zones. Permeability and specific yield/storage exhibit similar depth trends. While in the upper 200 mbgs fracture flow varies between confined and unconfined, we observe confined fracture and matrix flow below about 600 mbgs depth. The most important geological factors are current seismotectonic activity (determined by peak ground acceleration) and long-term tectonogeological history (determined by geological province). The impact of lithology is less important. Based on the regression coefficients derived for all the geological key factors, permeability ranges of crystalline rocks at site scale can be predicted. First tests with independent data sets are promising.

1. Introduction

Understanding and predicting the hydraulic properties of fractured crystalline rocks at site scale has high practical relevance and economic importance within the context of, for example, the production of hydrothermal and petrothermal energy, groundwater resources, earthquake science, geological waste disposal, mining, ore body formation, and underground constructions. Although hydraulic tests have been performed all over the world for some decades [e.g., Balla and Molnár, 2004; Brace, 1978; Gale, 1982; Lawson, 1968; Lomize, 1951; Manning and Ingebritsen, 1999; Maréchal et al., 2004; Masset and Loew, 2010; Stober and Bucher, 2007], our capability to predict hydraulic conditions in fractured rocks is still very limited [Berkowitz, 2002; Ingebritsen and Manning, 2010].

Hydrogeological data are often focused on specific sites, and some authors have compiled and generalized these data sets. For example, Freeze and Cherry [1979] and Brace [1980] derived general ranges of permeability for certain rock types. Permeability or hydraulic conductivity versus depth regressions on single-site or multisite data sets have been performed by, e.g., Carlsson and Olsson [1985], Davis and Turk [1964], Ingebritsen and Manning [1999], Lawson [1968], Ranjam et al. [2015], Snow [1968], or Stober and Bucher [2007]. Governing physical processes were inferred based on these regressions [e.g., Ingebritsen and Manning, 2003; Ishii, 2015; Jiang et al., 2010; Rutqvist, 2015; Rutqvist and Stephansson, 2003] and global maps of shallow permeability have been compiled based on lithology [Gleeson et al., 2014, 2011].

Controls on site-scale permeabilities can be roughly separated into technical and geological factors. Technical factors relate to the measurement method [e.g., Butler and Healey, 1998; Heitfeld et al., 1998; Prinz and Strauß, 2012; Scibek et al., 2016; Steiner et al., 2006], the tested interval length and its orientation, the radius of influence, or the tested rock volume [e.g., Clauser, 1992; Follin and Stigsson, 2014; Guéguen et al., 1996; Illman and Tartakovsky, 2006; Mattila and Tammisto, 2012; Nastev et al., 2004; Rumble, 1994;

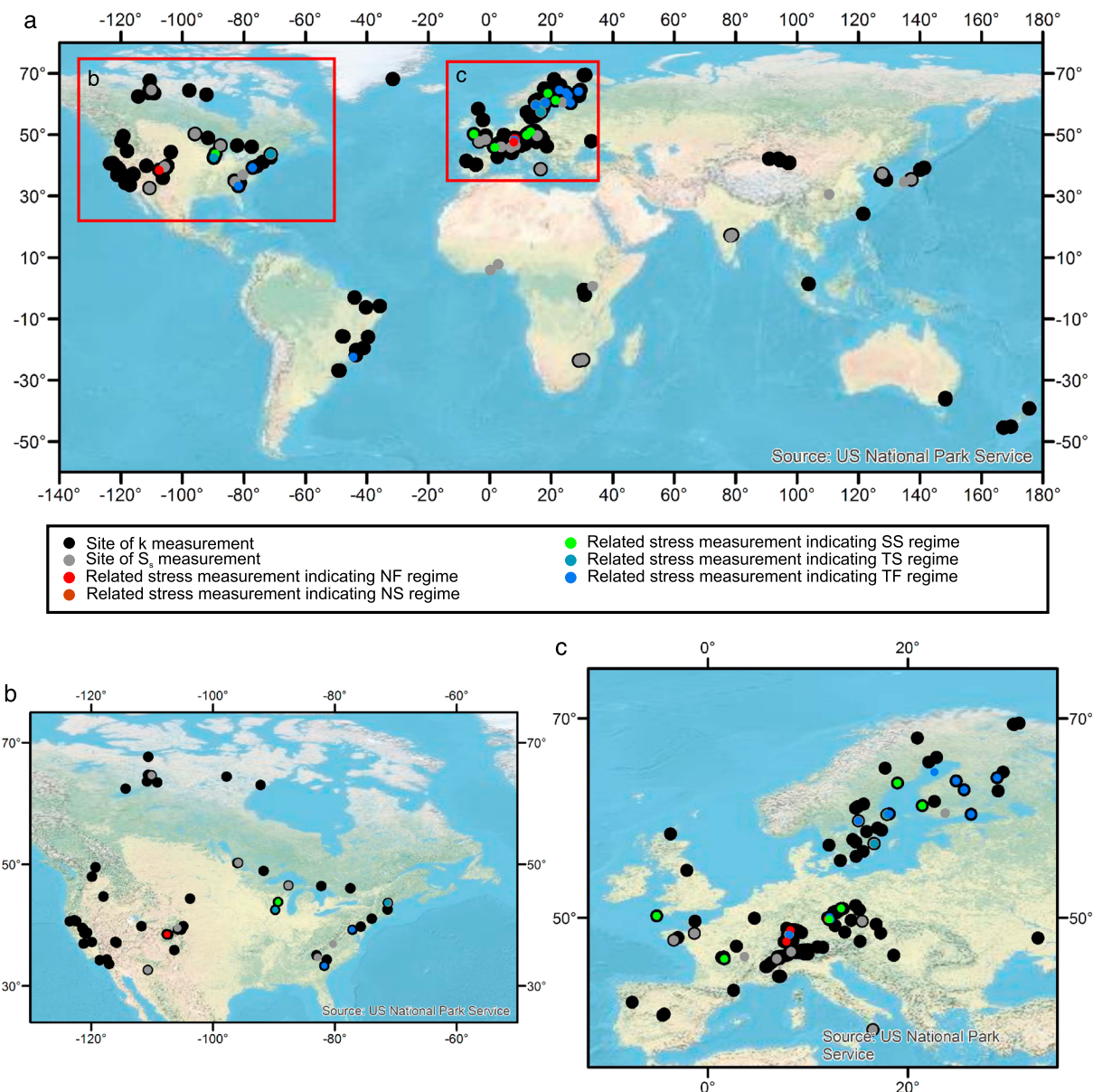


Figure 1. (a) World sites of permeability, specific storativity, and stress measurement. (b) Zoom of North American sites. (c) Zoom of European sites.

[Schulze-Makuch et al., 1999; 1998; Shapiro et al., 2015; Winkler and Reichl, 2014; Zimmermann et al., 2003; Zlotnik et al., 2000]. The nature and distribution of fractures is the most important geological factor determining permeability distribution at site scale in crystalline basement, as fractures provide secondary porosity and connectivity [e.g., Long et al., 1996]. Other factors influencing fluid flow in fractured rock are the thermo-hydro-chemo-mechanical (THCM) properties of the host rock, and in situ stress conditions [e.g., Bense et al., 2013; Ingebritsen and Gleeson, 2015; Mickelthwaite et al., 2010; Rutqvist and Stephansson, 2003; Stober and Bucher, 2015]. Less research has been performed on the influence of larger-scale geological processes and conditions such as contact or regional metamorphism [Achtziger-Zupančič et al., 2017; Baudoin and Gay, 1996; Matter et al., 2005], regional stress regime [Faulkner and Armitage, 2013], seismotectonic activity [e.g., Cox et al., 2014; Kitagawa et al., 2007; Manga et al., 2012; Wang and Manga, 2010] or geological history [Ranjram et al., 2015].

Here we present and analyze a unique worldwide compilation of about 29,000 in situ permeability measurements from crystalline rocks to depth of 2000 meters below ground surface (mbgs). We explore the influence

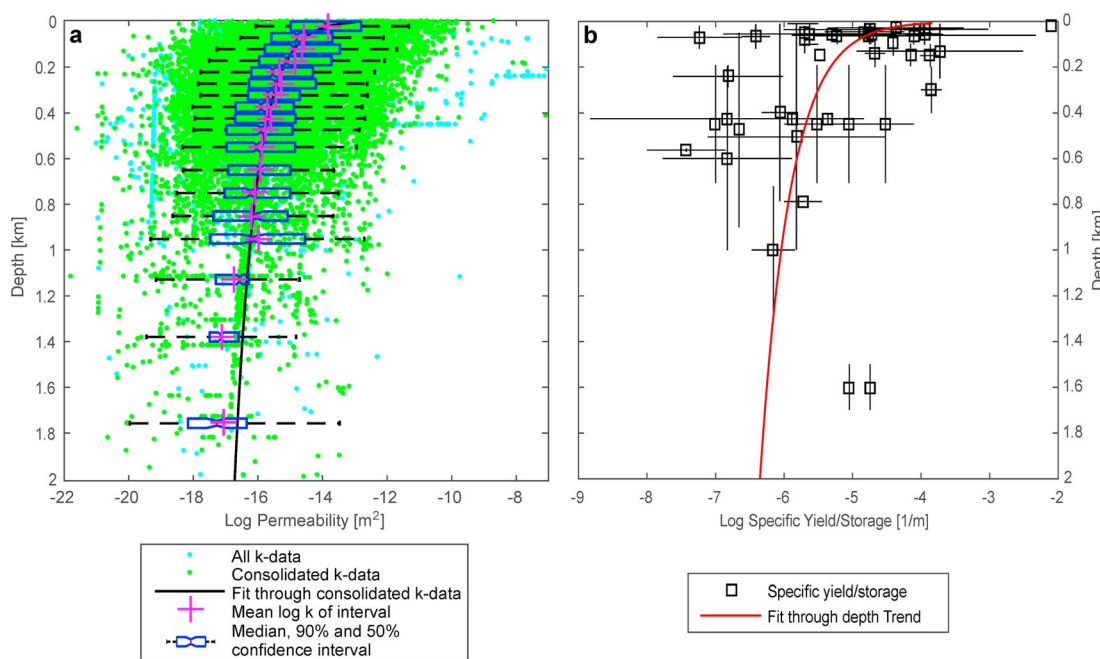


Figure 2. The depth trend of (a) permeability and (b) specific yield or storage, mean log (black square) with ranges of values (horizontal bar) and depth range (vertical bar) as derived from the site-specific references.

of method-related effects and large-scale geological processes by means of multivariate hypothesis testing. The analysis focuses on methodological factors such as the measurement method, measurement scale, and preferential sampling, and on geological factors such as the long-term geological history and its imprinted structural inventory, rock mass composition, current seismotectonic activity, and current local stress field. The data set shows that the permeability-depth relation depends on geological history, seismotectonic activity, and to a lesser extent lithology. A prediction procedure is developed based on a series of observed empirical log-log linear permeability-depth relationships. First applications of these relationships to new sites show a good correspondence with measured permeability ranges.

2. Data Processing

2.1. Data Compilation, Homogenization, and Consolidation

In this study, publicly available measurements of transmissivities, hydraulic conductivities, and permeabilities in crystalline basement rocks are compiled from tables and figures published in 221 journals, reports, and databases around the world (Figures 1 and 2a). These data are supplemented by unpublished data from mining and tunneling activities. The 28,832 estimates of hydraulic properties are based on in situ measurements carried out in the context of a wide range of geoscientific applications, such as geothermal energy, tunneling and mining, groundwater supply, siting or characterization of spent fuel and liquid waste disposal sites, and hydropower dams (Figure 2a and Figure S1 in the supporting information). Although this is a worldwide data compilation, consolidating data from several hundred sites situated in 30 countries (Figure 1), a large proportion of measurements originates from Europe (83% of all measurements) and North America (7%), supplemented by some major data sets from Japan, South Korea, and China (in total 7%), and only minor data sets from the rest of the world (3%).

Besides hydraulic properties, depth range, and length of tested intervals, a rough orientation of the measurement section (horizontal, oblique, and vertical), borehole radius, tested rock volume, radius of influence, and type of measurement have been extracted from the literature whenever possible. Temperature gradients or temperature measurements at or near these sites have been extracted from 102 mostly independent references. Missing temperature values have been calculated from a standard temperature gradient of 3E-2 K/m and the surface temperature for 179 shallow hydraulic measurements. Specific yield and

specific storage values are compiled from 32 sets of mainly cross-borehole hydraulic tests performed at 26 sites, mainly situated in granitic rocks at depths of up to 1700 mbgs (Figure 2b).

Due to the variety of data sources, transmissivity, hydraulic conductivity, and permeability were reported in various units including metric (m, m^2), Anglo-American (ft, ft^2, gpd) or other units ($D, Lugeon, Meinzer's unit$). All data have been converted to SI units, and transmissivity was normalized by the measurement interval length to yield hydraulic conductivity K in m/s , from which permeability k in m^2 has been estimated using

$$k = K \times \left(\frac{\mu}{\rho \times g} \right) \quad (1)$$

where μ is the dynamic viscosity of water in $kg/(m s)$, ρ is the density of the fluid in kg/m^3 , and g is the gravitational constant $9.81 m/s^2$. The estimation of density and dynamic viscosity and underlying assumptions are described in Appendix A. Hydrostatic pressure conditions in a fully saturated aquifer are assumed for most measurements. The major uncertainty in the permeability conversion stems from the fluid density and viscosity estimations. Based on a maximum temperature gradient error of $10 K/km$ and maximum total dissolved solids (TDS) in excess of $30 kg/m^3$ at deeper sites [Bucher and Stober, 2010; Frape and Fritz, 1987; Gascoyne et al., 1987; Ranjram et al., 2015; Stotler et al., 2010; Vovk, 1987], the error in the permeability calculated from hydraulic conductivity is negligible for low temperature and mineralization (shallow groundwater) and increases to about 20–25% for high temperatures and TDS [Kuder, 2011; Kwak et al., 2005].

We restricted our analysis to a depth range between 0 and 2000 mbgs, because there is an absolute scarcity of deeper in situ data. Permeabilities at or below the measurement limit are discarded, since these values reflect the physical limitations of each method. Data derived from intervals longer than 100 m are generally also discarded, as the boundary conditions for deriving these permeabilities are averaged over excessively large rock sections.

The hydraulic data stem from a wide range of test methods, which can roughly be grouped in hydraulic borehole measurements (open hole tests, single-packer and multipacker tests, Lugeon/WD tests, drill stem tests, flow meter logs, and hydraulic tests during or after hydraulic stimulation), pneumatic borehole measurements, pressure tests in tunnels, analysis of discrete tunnel inflow measurements, and indirect determinations of permeability from hypocenter movements of (induced) seismicity and calibrated groundwater flow models (using isotopes, temperature, etc). When computing statistics, a minimum of about 100 observations is regarded as being representative for a given property, and measurement methods with fewer observations (Table 1) have been removed from the analyses. Permeabilities estimated from stimulation tests have also been discarded, because it often remains uncertain whether the measurements relate to the natural or stimulated rock mass [e.g., Delisle, 1975; West et al., 1975]. Tracer test data are also discarded, as these tests often infer the permeability of single fractures from numerical and analytical solutions, which in turn are based on an uncertain estimation of the rock properties controlling the flow velocity. The resulting reduced database is shown in Figure 2a, and we refer to it as “consolidated” database.

2.2. Specific Storage and Calculated Test Volume

Specific yield and specific storage values ($S_{y/s}$), ranging from $2E-9$ to $5E-3$ have been compiled from cross-hole hydraulic tests or time transient models (32 values) over the same depth range as the permeabilities (Figure 2b). Both measures are collated, as a simple distinction is often impossible. Sometimes references report different values for a single site (e.g., Illman et al. [2009], Japan Nuclear Cycle Development Institute (JNC) [2000], and Zha et al. [2015] at Mizunami Lab/Tono Mine, Japan), which are then treated as independent measures. Whenever more than one value was reported in a reference, averages between extreme values have been calculated.

The specific yield or storage values decrease from about $1E-3$ close to the surface to about $1E-6$ at 1000 mbgs. A log-log linear regression has been fitted as $\log(S_{y/s}) = -1.0 \times \log(z) - 6.0$ (z in km). Therefore, the specific storage roughly changes by 1 order of magnitude per order of magnitude depth change and the specific storage at 1000 mbgs typically equals $1E-6$, a value frequently used in hydrogeological subsurface models [e.g., Masset and Loew, 2010].

Table 1. Hydraulic Test Types Contributing to the Database of This Study

Test Method	Log Permeability-Literature (m ²) ^a			Log Permeability-Data Set (m ²)			
	Min	Max	Min	Mean	Max	Observations	
Measurement-based aquifer scale model ^b	-20	-10	-16.5	-14.7	-13.2	37	
Discrete tunnel inflow measurement ^{c,d}	-20	-8	-21.8	-15.7	-8.7	2,870	
(Induced) seismicity ^e	-16	-7?	-16.0	-15.3	-14.9	3	
Cross-borehole tracer test ^f	-15	-8	-17.9	-10.9	-6.9	119	
Open hole pumping/slug test ^{f,g}	-14 to -13	-8	-17.7	-12.7	-9.9	687	
Single-packer test ^{f,g,h,i,j,k}	-21 to -14	-13 to -8	-20.9	-14.8	-7.1	773	
Multi-packer test ^{g,h,i,j,k}	-21 to -18	-13 to -8	-21.6	-15.5	-7.7	13,877	
Drill stem test ^{f,i,j,k,l,m}	-17 to -14	-13 to -11	-18.3	-17.0	-16.1	5	
Borehole Lugeon/WD test ^{f,i,m,n}	-18 to -15	-12 to -8	-18.0	-13.6	-9.1	334	
Difference flow logs ^o	-18	-13	-17	-15.1	-9.9	4,635	
Pneumatic test ^p	-21	-8	-21	-14.9	-13.0	64	
Pressure tunnel test	?	?	-15.7	-14.3	-12.9	14	
Hydrofrac test ^{g,h,i,j,k,l}	-21 to -18	-13 to -8	-18.5	-16.7	-14.2	45	

^a?, Uncertain/unknown.^bGleeson *et al.* [2011].^cAchtziger-Zupančič *et al.* [2017].^dMasset and Loew [2010].^eIngebritsen and Manning [2010].^fPrinz and Strauß [2012].^gSteiner *et al.* [2006].^hClauer [1991].ⁱHeitfeld *et al.* [1998].^jLee *et al.* [1982].^kLeech *et al.* [1984].^lAlmén *et al.* [1986].^mDenzel *et al.* [1997].ⁿSievänen [2001].^oLudvigson *et al.* [2002].^pAuthors experience.

The tested rock mass volume is rarely estimated and reported in the literature (263 measurements). Therefore, we calculated the tested rock volume V in m³ as the volume of a cylinder around the tested interval:

$$V = \pi \times R_i^2 \times l \quad (2)$$

where l in m is the length of the measurement interval and R_i in m is the radius of influence of the hydraulic test. For confined aquifers the radius of influence is mainly dependent on the amount of water flowing into or out of the test section [Black *et al.*, 1987]. As the water volume equals the flow rate over a certain time, the test time t in s (or an estimate) was compiled whenever reported. For constant head and constant rate tests, the radius of influence has been estimated according to Jacob and Lohman [1952]:

$$R_i = \sqrt{\frac{2.25 \times K \times t}{S_s}} \quad (3)$$

where K is the hydraulic conductivity and S_s is the depth-dependent specific storage as approximated from the global depth regression. In slug tests, the injected or extracted water volume, and thus the radius of influence, is defined by the water stored in the test rod and can be approximated by Cooper *et al.* [1967]:

$$R_i = \frac{r_c/e}{\sqrt{S_s \times l}} \quad (4)$$

where r_c is the inner radius of the test rod, which is assumed to be 25.4 mm (1") as the test rods are usually 2" in diameter. In pulse tests, the equivalent radius r_e in meters results from the compliance of the system which

Table 2. Permeability/Depth Summary of the Entire Data Set and Sub-Data Sets

	Measurements	Log Permeability (m^2)			Depth Range (mbgs)		
		Min	Max	Regions	Countries	Min	Max
Entire data set	19,062	-21.8	-7.1	128	27	1	1,980
Nongeological factors							
Method							
Borehole Lugeon/WD test	328	-17.8	-9.1	20	6	2	981
Discrete tunnel inflow measurement	2,797	-21.8	-8.7	7	5	1	1,866
Multipacker test	11,182	-21.6	-7.7	80	21	1	1,973
Difference flow log	3,570	-16.9	-9.9	7	5	5	1,151
Open hole pumping/slug test	526	-17.7	-10.1	21	14	3	421
Single-packer test	659	-20.9	-7.1	27	10	1	1,980
Log test length (m)							
-1 to 0	394	-19.9	-11.5	11	7	1	1,277
0-1	10,077	-21.6	-7.7	61	20	1	1,888
1-2	8,197	-21.8	-7.1	90	22	1	1,980
Orientation (deg)							
Horizontal 0–30	3,747	-21.8	-8.7	18	9	1	1,866
Oblique 30–60	2,778	-21.0	-7.7	15	6	5	947
Vertical 60–90	12,275	-21.6	-7.1	110	27	1	1,980
Log tested rock volume (m^3)							
-6 to -5 borehole inflows	1	-19.9	-19.9	1	1	68	68
-5 to -4 borehole inflows	2	-19.3	-19.2	1	1	127	128
-4 to -3 borehole inflows	54	-19.2	-17.2	1	1	15	365
-3 to -2 borehole inflows	242	-20.4	-13.4	7	5	4	524
-2 to -1 borehole inflows	1,456	-20.4	-11.3	12	7	5	870
-1 to 0 borehole inflows	2,149	-21.6	-9.8	20	10	1	1,498
0-1 borehole inflows	2,073	-20.3	-10.3	32	13	2	1,818
1-2 borehole inflows	2,169	-19.4	-9.5	46	15	3	1,940
2-3 borehole inflows	2,062	-20.8	-10.4	56	17	4	1,843
3-4 borehole inflows	893	-20.9	-11.0	42	16	9	1,973
4-5 borehole inflows	442	-20.1	-7.1	25	14	10	1,980
5-6 borehole inflows	189	-15.3	-9.9	23	12	10	971
6-7 borehole inflows	63	-18.6	-9.1	13	9	24	721
7-8 borehole inflows	12	-18.6	-8.1	6	4	27	617
8-9 borehole inflows	10	-11.0	-7.7	3	3	43	187
9-10 borehole inflows	11	-13.6	-9.8	3	3	40	421
-4 to -3 drift inflows	1	-21.0	-21.0	1	1	231	231
-3 to -2 drift inflows	4	-21.0	-19.9	1	1	231	425
-2 to -1 drift inflows	2	-20.3	-20.1	1	1	234	426
0-1 drift inflows	1	-21.8	-21.8	1	1	1,110	1,110
1-2 drift inflows	1	-20.7	-20.7	1	1	1,810	1,810
2-3 drift inflows	5	-20.2	-19.3	1	1	1,110	1,410
3-4 drift inflows	22	-19.3	-17.1	1	1	141	1,630
4-5 drift inflows	450	-18.5	-14.3	3	2	4	1,866
5-6 drift inflows	1,505	-17.5	-13.8	4	3	7	1,810
6-7 drift inflows	351	-16.6	-13.1	3	2	14	1,810
7-8 drift inflows	329	-16.8	-12.1	2	2	12	1,810
8-9 drift inflows	50	-14.8	-12.1	2	2	65	1,304
9-10 drift inflows	53	-14.9	-8.7	1	1	1	1,416
10-11 drift inflows	2	-12.8	-12.7	1	1	262	285
11-12 drift inflows	1	-12.0	-12.0	1	1	1,100	1,100
Geological factors							
Lithology							
Metamorphic rocks							
Marble	682	-20.2	-10.4	6	5	7	1,193
Quartzite	122	-18.7	-11.8	4	4	3	1,193
Contact	1,433	-21.8	-9.9	9	5	6	1,866
Intermediate-grade	2,446	-21.8	-9.9	23	12	3	1,866
High-grade	6,790	-20.2	-8.7	37	14	1	1,680
Ultra-high-grade	2,984	-20.2	-8.7	17	8	1	1,680
Metaintrusive	8,685	-21.6	-7.7	46	13	1	1,680
Metavolcanic	6,745	-18.8	-9.8	29	8	1	1,680

Table 2. (continued)

	Measurements	Log Permeability (m^2)		Regions	Countries	Depth Range (mbgs)	
		Min	Max			Min	Max
Intrusion							
Acidic	15,957	-21.8	-7.1	77	23	1	1,980
Intermediate	3,367	-20.9	-10.9	13	9	4	1,980
(Ultra-) Basic	1,566	-18.9	-10.9	9	5	4	931
Geological province							
Basin	629	-20.3	-7.1	5	4	5	1,980
Extensional	217	-17.3	-12	4	2	3	420
Orogen							
Collisional	1,758	-18.7	-8.7	11	5	1	1,680
Passive	3,072	-21.8	-9.8	31	9	3	1,866
Subduction	1,076	-19.1	-9.8	24	5	1	1,241
Stable	12,310	-21.6	-7.7	53	11	1	1,269
Peak ground acceleration (m^2/s)							
Very low hazard 0–0.2	10,814	-21.6	-7.7	41	8	1	1,269
Low hazard 0.2–0.8	4,479	-21.8	-9.8	47	16	3	1,980
Moderate hazard 0.8–2.4	3,145	-20.3	-7.1	36	14	1	1,680
High hazard >2.4	531	-19.0	-9.8	7	4	3	1,241
Local stress regime							
Normal faulting	85	-17.5	-10.9	3	3	2	250
Oblique normal faulting	2	-16.9	-16.2	1	1	148	150
Strike-slip faulting	2,221	-18.3	-11.0	7	6	1	1,410
Thrust faulting	3,720	-19.9	-7.7	13	5	3	987
Oblique thrust faulting	372	-19.0	-10.1	6	3	7	987

is determined by the total volume of water involved per unit of head change [Black *et al.*, 1987] and is calculated by Bredehoeft and Papadopoulos [1980]

$$r_e = \sqrt{\frac{C \times \rho \times g}{\pi}} \quad (5)$$

where C is the system compressibility (defined by the compressibility of the test system and the compressibility of water in the test interval), which is approximated as $2.4\text{E}-9 \text{ Pa}^{-1}$ [Steiner *et al.*, 2006; Stevenson *et al.*, 1996].

Most of the compiled measurements can be attributed to constant head or constant rate tests, slug tests, or pulse tests. Often, critical inputs (e.g., testing time) could not be derived from the reports, and therefore, the test volume has only been approximated for about half of the consolidated database.

2.3. Separation Into Sub-Data Sets

To assess the influence of depth on permeability, the database is divided into measurement depth intervals of 50 m for depths ranging from 0 to 500 mbgs, 100 m intervals for 500 to 1000 mbgs, 250 m intervals for 1000 to 1500 mbgs, and one single interval for 1500 to 2000 mbgs. The database is also subdivided (Table 2) according to permeability measurement methods (six classes), orientation of the test section (three classes), order of magnitude of the interval length (three classes), order of magnitude of the tested rock volume (18 classes), lithology (11 classes), geological provinces (six classes), peak ground acceleration (PGA, four classes), and local stress regime (five classes).

2.4. Multiple Regression Analysis and K-Means Clustering

Statistical moments are calculated for each sub-data set based on geological factors that contain at least 50 observations (Figures 3a–3c). The k-means algorithm [Arthur and Vassilvitskii, 2007; Lloyd, 1982] clusters data according to the Euclidean distance of the mean log, log variance, and log skewness of the permeability distribution in each depth interval and for each factor. The number of clusters are defined by a silhouette plot

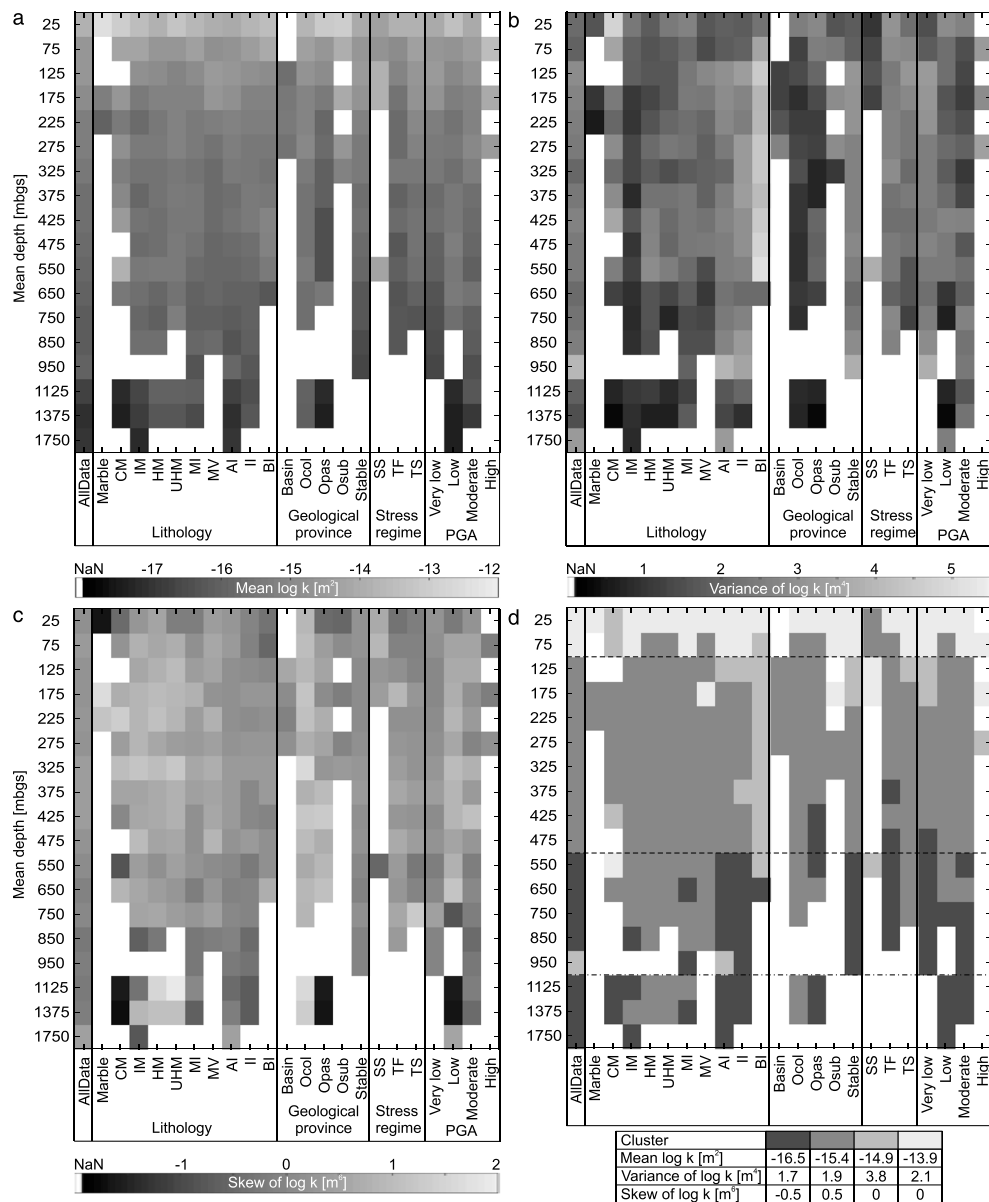


Figure 3. (a) Log mean permeability, (b) variance of the permeability distribution, and (c) skew of the permeability distribution shown for sufficiently populated permeability subdata sets defined by the depth intervals and the geological properties. White indicates subdata sets with fewer data than the minimum entity (50 observations). (d) The result of k-means clustering based on the statistical moments shown in Figures 3a–3c; CM, contact metamorphic; IM, intermediate-grade metamorphic; HM, high-grade metamorphic; UHM, ultra-high-grade metamorphic; MV, metavolcanic; MI, metatrustive; AI, acidic intrusive; II, intermediate intrusive; BI, basic intrusive; Opas, passive orogen; Ocol, continent-continent collisional orogen; Osub, subduction-related orogen; SS, strike-slip regime; TF, thrust fault regime; TS, oblique thrust fault regime; PGA, peak ground acceleration.

algorithm [Kaufman and Rousseeuw, 1990], showing four clusters to be most suitable. Figure 3d displays parameters related to the centroid of each cluster.

A linear regression of log permeability ($\log k$) over log depth ($\log z$) is performed on the entire data set and the sub-data sets including more than 100 observations. Each regression follows the equation $\log(k) = A \times \log(z) + B$ with depth in kilometers being positive (Table 3). A is called the slope value or simply slope and B is the intercept (defining the permeability at 1000 mbgs). In this study, we define a “steep slope” of the regression as a mathematically low slope value and accordingly a “small slope” as a higher slope

Table 3. Regression Parameters for the Factors Shown in Figures 5 and 7^a

	Regression 0–2000 mbgs								Regression 0–1000 mbgs				
	Data Set				Mean		Median		Data Set				
	A	B	R ²	RMSE	A	B	A	B	A	B	R ²	RMSE	
Entire data set													
Mean log K	−1.53	−16.26	0.20	1.54	−1.75	−16.40	−1.66	−16.48	−1.46	−16.18	0.17	1.54	
Data within the lower 10% quantile	−1.78	−18.90	0.63	0.64	NaN	NaN	NaN	NaN	−1.71	−18.90	0.59	0.63	
Data within the upper 10% quantile	−1.24	−13.20	0.49	0.67	NaN	NaN	NaN	NaN	−1.11	−13.10	0.45	0.63	
Nongeological factors													
Method													
Borehole Lugeon/WD test	−1.31	−15.57	0.23	1.04	NaN	NaN	NaN	NaN	−1.31	−15.57	0.23	1.04	
Discrete tunnel inflow measurement	−1.10	−16.26	0.21	0.98	−1.09	−16.22	−0.96	−16.38	−0.73	−15.94	0.09	0.94	
Multipacker	−1.59	−16.37	0.13	1.71	−1.90	−16.65	−2.04	−16.85	−1.52	−16.30	0.12	1.70	
Difference flow log	−0.50	−15.13	0.04	1.17	−0.53	−15.19	−0.45	−15.34	−0.50	−15.13	0.04	1.17	
Open hole pumping/slug test	−1.36	−14.45	0.14	1.00	NaN	NaN	NaN	NaN	−1.36	−14.45	0.14	1.00	
Single-packer test	−1.20	−15.82	0.20	1.57	−1.29	−15.71	−1.60	−16.17	−1.19	−15.81	0.20	1.53	
Log test length (m)													
−1 to 0	−0.80	−15.41	0.04	1.08	NaN	NaN	NaN	NaN	−0.76	−15.38	0.04	1.08	
0–1	−1.16	−16.08	0.12	1.48	−1.17	−16.08	−1.00	−16.04	−1.15	−16.07	0.12	1.48	
1–2	−2.08	−16.48	0.30	1.58	−2.15	−16.52	−2.10	−16.63	−2.00	−16.40	0.25	1.60	
Orientation (deg)													
Horizontal 0–30	−1.69	−16.25	0.24	1.32	−1.54	−16.24	−1.34	−16.37	−1.41	−16.01	0.13	1.35	
Oblique 30–60	−1.35	−16.56	0.13	1.48	−1.21	−16.42	−0.99	−16.20	−1.35	−16.56	0.13	1.48	
Vertical 60–90	−1.56	−16.22	0.20	1.60	−1.90	−16.46	−1.84	−16.49	−1.51	−16.16	0.19	1.58	
Log tested rock volume (m ³)													
−3 to −2 borehole inflows	−1.90	−19.23	0.66	0.51	NaN	NaN	NaN	NaN	−1.90	−19.23	0.66	0.51	
−2 to −1 borehole inflows	−1.95	−18.13	0.60	0.72	−2.02	−18.2	−2.08	−18.18	−1.95	−18.13	0.60	0.72	
−1 to 0 borehole inflows	−1.90	−17.36	0.45	0.99	−1.98	−17.46	−2.28	−17.74	−1.89	−17.36	0.45	0.99	
0–1 borehole inflows	−1.83	−16.87	0.37	1.20	−1.61	−16.66	−1.68	−16.64	−1.72	−16.76	0.34	1.17	
1–2 borehole inflows	−1.64	−16.28	0.36	1.09	−1.60	−16.14	−1.46	−16.08	−1.54	−16.15	0.34	1.06	
2–3 borehole inflows	−1.37	−15.59	0.16	1.32	−1.40	−15.59	−1.26	−15.40	−1.35	−15.57	0.15	1.32	
3–4 borehole inflows	−2.32	−15.90	0.40	1.50	−1.57	−15.01	−1.24	−14.71	−2.14	−15.70	0.36	1.43	
4–5 borehole inflows	−1.46	−14.10	0.38	0.84	NaN	NaN	NaN	NaN	−1.43	−14.07	0.36	0.78	
5–6 borehole inflows	−1.12	−13.06	0.24	0.84	NaN	NaN	NaN	NaN	−1.12	−13.06	0.24	0.84	
4–5 drift inflows	−1.29	−17.26	0.92	0.24	−1.30	−17.32	−1.24	−17.25	−1.14	−17.09	0.85	0.22	
5–6 drift inflows	−1.18	−16.57	0.78	0.25	−1.14	−16.55	−1.04	−16.45	−1.09	−16.49	0.71	0.24	
6–7 drift inflows	−1.31	−15.63	0.76	0.34	NaN	NaN	NaN	NaN	−1.23	−15.56	0.70	0.35	
7–8 drift inflows	−2.07	−15.57	0.56	0.77	NaN	NaN	NaN	NaN	−1.49	−15.14	0.36	0.72	
Geological Factors													
Lithology													
Metamorphic rocks													
Marble	−2.41	−16.78	0.55	1.25	−3.60	−18.19	−4.02	−18.71	−2.40	−16.77	0.55	1.25	
Quartzite	−1.48	−15.58	0.26	1.36	NaN	NaN	NaN	NaN	−1.39	−15.49	0.24	1.34	
Contact	−2.22	−16.34	0.31	1.70	−2.05	−16.13	−2.18	−16.49	−1.43	−15.59	0.11	1.78	
Intermediate grade	−1.79	−16.40	0.43	1.21	−1.76	−16.36	−1.65	−16.5	−1.63	−16.23	0.32	1.25	
High grade	−1.36	−16.13	0.22	1.33	−1.23	−16.04	−1.22	−16.33	−1.38	−16.16	0.21	1.34	
Ultrahigh grade	−1.45	−16.00	0.23	1.37	−1.32	−15.92	−1.44	−16.33	−1.46	−16.01	0.20	1.4	
Metaintrusive	−1.49	−16.18	0.17	1.48	−1.53	−16.19	−1.57	−16.36	−1.50	−16.19	0.16	1.49	
Metavolcanic	−1.37	−16.14	0.19	1.40	−1.42	−16.19	−1.18	−16.23	−1.38	−16.15	0.18	1.40	
Intrusion													
Acidic	−1.43	−16.17	0.16	1.55	−1.69	−16.36	−1.58	−16.41	−1.33	−16.07	0.13	1.56	
Intermediate	−1.53	−16.20	0.10	1.66	−1.49	−16.17	−1.58	−16.37	−1.47	−16.16	0.08	1.68	
(Ultra) Basic	−1.44	−16.06	0.06	2.03	−1.58	−16.13	−2.22	−16.77	−1.44	−16.06	0.06	2.03	
Geological Province													
Basin	−1.87	−16.79	0.19	1.79	0.30	−15.31	0.17	−15.52	−1.38	−16.38	0.09	1.68	
Orogen													
Collisional	−1.36	−15.94	0.27	1.07	−1.34	−15.93	−1.25	−16.38	−1.36	−15.94	0.23	1.10	
Passive	−2.34	−17.07	0.45	1.35	−2.23	−16.99	−2.43	−17.27	−2.35	−17.08	0.38	1.40	
Subduction	−1.44	−15.60	0.23	1.52	−1.72	−15.71	−1.87	−15.79	−1.44	−15.60	0.23	1.52	
Stable	−1.35	−16.12	0.14	1.60	−1.65	−16.36	−1.56	−16.38	−1.33	−16.10	0.13	1.59	

Table 3. (continued)

	Regression 0–2000 mbgs								Regression 0–1000 mbgs				
	Data Set				Mean		Median		Data Set				
	A	B	R ²	RMSE	A	B	A	B	A	B	R ²	RMSE	
Peak ground acceleration (m ² /s)													
Very low hazard	0–0.2	−1.48	−16.26	0.16	1.59	−1.75	−16.48	−1.69	−16.50	−1.46	−16.24	0.15	1.58
Low hazard	0.2–0.8	−1.81	−16.49	0.28	1.47	−1.89	−16.48	−1.89	−16.76	−1.61	−16.27	0.20	1.49
Moderate hazard	0.8–2.4	−1.41	−16.17	0.26	1.37	−1.59	−16.27	−1.42	−16.41	−1.35	−16.11	0.22	1.36
High hazard	>2.4	−1.23	−15.28	0.08	1.78	−1.81	−15.52	−2.12	−15.74	−1.23	−15.28	0.08	1.78
Stress regime													
Thrust faulting		−1.49	−16.50	0.11	1.60	−1.51	−16.50	−1.74	−16.69	−1.49	−16.50	0.11	1.60
Oblique thrust faulting		−1.68	−16.19	0.11	1.54	−1.60	−16.18	−1.77	−16.28	−1.68	−16.19	0.11	1.54

^aNaN, insufficient data.

value (closer to 0). The predictive capability is assessed by the goodness of fit R^2 . The root-mean-square error (RMSE) describes the mean distribution of the data around the regression at any given depth.

3. Technical Factors Controlling Permeability Distributions

3.1. Sampling Bias and Limitations of the Test Methods Considered

The analysis of the influence of the method itself on the permeability measurement is carried out for the six methods with sufficient observations (open hole tests, single-packer and multipacker tests, flow meter logs, borehole Lugeon/WD tests, and discrete tunnel inflow measurements; Figure S2). Most of these methods rely on analytical solutions for radial flow to a borehole or cylindrical excavation in a homogeneous and isotropic aquifer.

Hydraulic tests with single-packer and multipacker systems are often conducted in less fractured and lower permeability rock masses in the upper 1000 mbgs that are studied for characterization of geological disposal sites for radioactive and chemical wastes or geothermal applications [e.g., JNC, 2000; Mather and Sargent, 1986; McEwen and Äikäs, 2000; Thury *et al.*, 1994; Wang *et al.*, 2006]. Based on high-quality flow rate and pressure monitoring data, diagnostic plots and heterogeneous flow models with various types of inner and outer boundary conditions [Horne, 1995; Kruseman and de Ridder, 1991] can be applied to the analysis of such packer test data. Thus, packer test results can have a very high accuracy and cover a wide permeability range, as shown by the compiled data set [Table 1; Almén *et al.*, 1986; Clauser, 1991; Heitfeld *et al.*, 1998; Lee *et al.*, 1982; Leech *et al.*, 1984; Prinz and Strauß, 2012; Steiner *et al.*, 2006].

For ground water exploration, typically more transmissive fracture networks are prospected in more or less shallow, open wells [e.g., Stober, 1997; Zeitlhöfer *et al.*, 2015]. The quality of these test results is a function of the devices used to control flow rate and pressure drawdown, as well as the length and natural head distribution along the open well. Our database shows a wider range of permeabilities (1E–10 to 2E–18 m²) than that specified in the literature (1E–8 and 1E–14 m², Tables 1 and 2), demonstrating that in practice this method characterizes all parts of the rock mass (matrix, fractures, and disintegrated rock).

For more detailed analysis of waste disposal sites, the hydraulic characterization of preferential groundwater flow and pollutant migration paths is a critical task [e.g., Ahokas *et al.*, 2013; Ludvigson *et al.*, 2002; Paillet *et al.*, 2012]. The location and transmissivity of conductive fractures can be determined using various types of flow logs and temperature profiling. The estimated fracture or interval transmissivity from these methods exhibits a larger error than packer tests due to uncertainties in fracture hydraulic head, flowrates, and the short testing time. The “difference flow logs” used in the Scandinavian nuclear waste disposal programs are restricted to flow rates of 0.1 ml/min to 5000 ml/min over small intervals (<2 m), resulting in a permeability range of 1E–18 to 5E–14 m² which is narrower than the compiled permeability ranges [e.g., Ahokas *et al.*, 2013; Ludvigson *et al.*, 2002; Pöllänen and Rouhiainen, 1998b] (Tables 1 and 2).

Lugeon or water pressure tests (WD-test from German “Wasserdruck-”) are mainly used in hydropower dam and tunnel projects and give a rough estimate of the hydromechanical properties of single fractures and

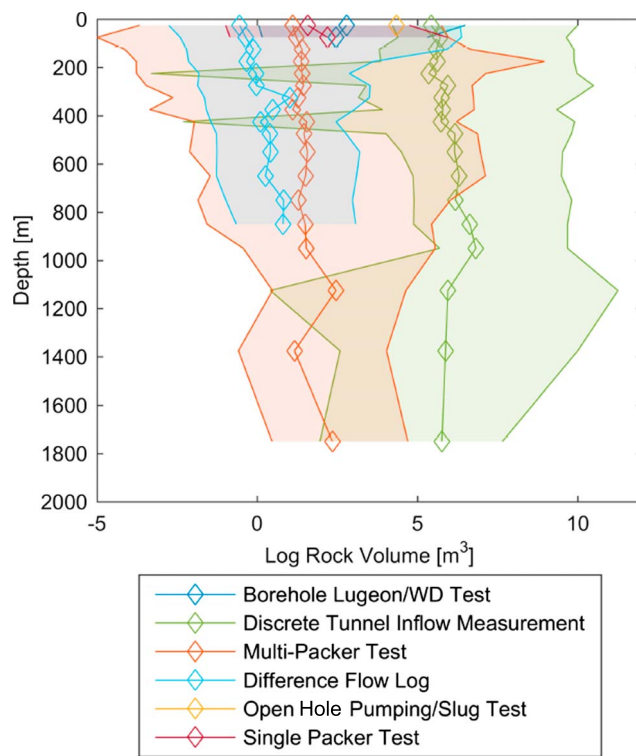


Figure 4. Depth trend of the mean log of the calculated rock test volume (diamonds) and the 90% confidence intervals (shaded areas) for the various hydraulic test methods.

mining sites, and galleries situated in the Swiss Alps and the Ore Mountains [Achtziger-Zupančič et al., 2017; Masset and Loew, 2010, 2013].

Thus, the various measurement methods represented in our database can capture different permeability ranges and are used for different purposes. Some measurement methods are restricted to certain ranges of depth and rock volumes and thus to certain parts of the rock mass. Differences in accuracy of derived permeability are related to the resolution of recorded and processed flow and pressure data, the chosen flow models, and duration of testing (Figures 4 and 5). The multipacker test is most widely used and its ranges of applicability encompass the other test methods.

3.2. Scale Effects

It has been postulated that permeability of crystalline rocks is dependent on measurement scale [e.g., Clauer, 1992; Nastev et al., 2004; Schulze-Makuch et al., 1999]. Our database includes sample and test interval lengths ranging between 0.1 and 100 m. Samples are grouped by logarithmic length magnitudes (0.1–1 m, 1–10 m, and 10–100 m). The sub-data sets are shown in Figure S3.

Following the procedure outlined in section 2.2, the calculated radius of influence ranges from 1E–3 and 1E5 m and the calculated rock test volumes from 1E–5 and 2E11 m³ (Figures 4, S4, and S5), resulting in 18 classes of log volume with most samples between 1E–2 and 1E6 m³ (Table 2). The calculated rock test volumes mainly depend on the permeabilities and geometrical factors of the test sections and are thus dependent measures of scale effects.

3.3. Preferential Sampling

In crystalline rocks, secondary pore space from fractures controls rock mass permeability [e.g., Long et al., 1996]. Close to the surface, sheet fractures can develop parallel to local topography due to exhumation and stress release [Mattila and Tammisto, 2012] and tectonic fractures open due to stress relaxation [Follin and Stigsson, 2014]. Deeper underground (>200 m), fractures are mainly (sub) vertically oriented [e.g., Boutt et al., 2010; Masset and Loew, 2013; Mazurek, 1998]. Therefore, the orientation of boreholes

fracture networks but less information about the hydraulics of the matrix and the entire rock mass. These tests are short term with a maximum depth of some hundred meters. Permeabilities are approximated by empirical solutions and are reported to range between 1E–18 and 1E–8 m² [Denzel et al., 1997; Heitfeld et al., 1998; Prinz and Strauß, 2012; Sievänen, 2001; Snow, 1979; Steiner et al., 2006], roughly agreeing with the compiled data (Tables 1 and 2).

Back analyses of discrete tunnel inflow measurements result in estimations of fracture transmissivity and isotropic or vertical rock mass permeabilities. Uncertainties relate to the simplification of analytical solutions used and uncertainties in measurement time, and specific storage and hydraulic head averaged over large rock mass volumes. Reported rock mass permeabilities range between 2E–22 and 2E–9 m² and are mainly derived from tunnels,

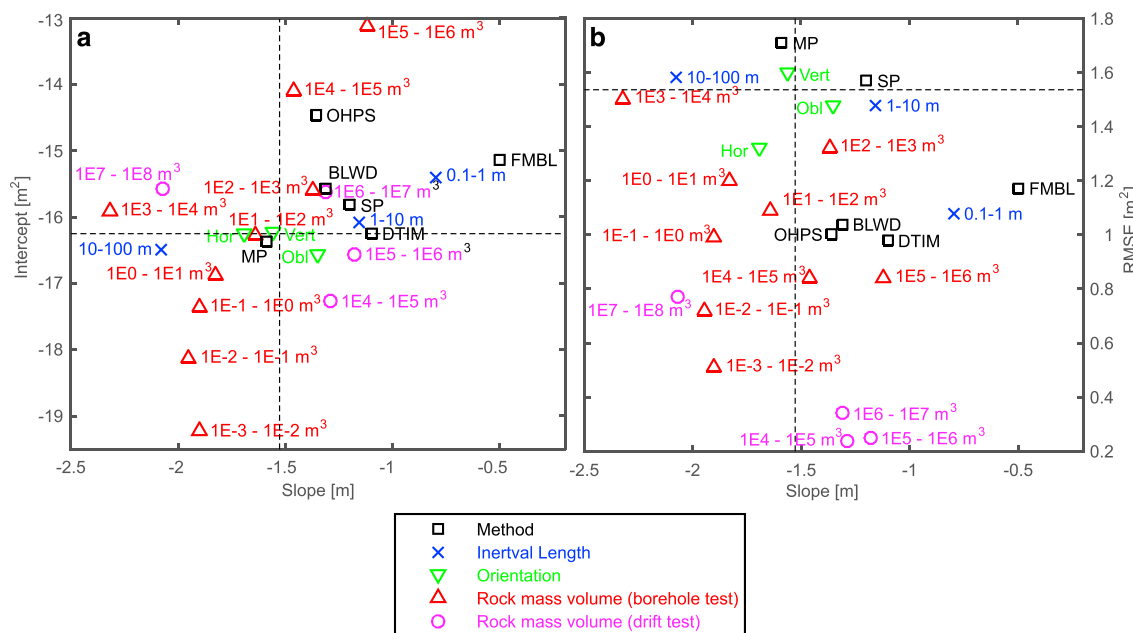


Figure 5. Parameters of regression through permeability measurements for sub-data sets defined by nongeological factors. BLWD, Borehole Lugeon/WD test; DTIM, discrete tunnel inflow measurement; FMBL, difference flow log; MP, multipacker test; OHPS, openhole pulse and slug tests; SP, single-packer test. The intersection of the dashed lines shows where the regression parameters of the entire data set plot. (a) Intercept versus slope of the regression. (b) Root-mean-square error (RMSE) versus the slope of the regression.

and underground excavations may influence the determined permeability distribution. The permeability measurements have been grouped into 30° intervals according to the inclination of the sampling section (borehole, tunnel, Figure S3). Most measurements were conducted in (sub) vertically (60–90° from horizontal) oriented test sections in boreholes drilled from the surface (Table 2). Oblique measurements were mainly sampled in boreholes for Swedish and Finnish site characterization. Horizontal sampling of permeabilities (0–30°) was mainly conducted in tunnels, galleries, and mines or in subhorizontal boreholes drilled from underground excavations. The ranges of permeability for these orientation classes invariably cover the entire spectrum of compiled permeabilities (Table 2).

4. Geological Factors Controlling Permeability Distribution

4.1. Lithology

In this study, intrusive and medium- to high-grade metamorphic rocks are considered crystalline basement rocks. Nonmetamorphic volcanic rocks are excluded from the analysis as they exhibit a wide range of hydraulic properties similar to sedimentary rocks. The influence of lithology on crystalline rock permeability is controversial: some authors state that lithology has only minor influence on rock mass permeability [e.g., *Davis and Turk*, 1964; *Winkler and Reichl*, 2014]. However, at some sites, crystalline rocks show systematic variations of hydraulic properties as a function of mineralogical composition [e.g., *Davies and Ó Dochartaigh*, 2002; *Gustafson and Krásny*, 1994; *Henriksen*, 2008; *Holland and Witthüser*, 2011; *Masset and Loew*, 2010; *Stober*, 1995]. In addition, the formation, propagation, and sealing of fractures in crystalline rocks is lithology and rock texture dependent [*Hoek and Diederichs*, 2006; *Hoek and Martin*, 2014; *Rawling et al.*, 2002; *Wong and Zhu*, 2013].

We compiled lithologic composition of the rock mass from the same references used for the compilation of hydraulic data. In case of questionable or incomplete lithological descriptions, geological information has been included from other sources such as geological maps. Different lithologies often appear closely related or interbedded. Lithological descriptions have therefore been generalized such that they describe entire boreholes or sites.

Some 60 different detailed descriptions of lithology were reported and merged into 11 genetic classes. As the bulk SiO₂ content defines the weathering behavior and mineralogical products [Mazurek, 1998, 2000], intrusive rocks have been separated into acidic intrusives (>63 m% SiO₂) including granites, granodiorites, pegmatites, and syenites; intermediate intrusives (52–63 m% SiO₂) such as diorites, monzonite, syenodiorites, gabbrodiorites, and basic and ultrabasic rocks like gabbro, anorthosite, dolerite, dunite, and norite (<52 m% SiO₂). However, exact separation of these rocks is difficult as they form mineralization series and thus are sometimes spatially closely related. The largest category in our database is acidic rocks, the smallest is basic and ultrabasic rocks (Table 2 and Figure S6).

The P-T conditions control rock mineralogy and structure during metamorphic overprint, especially in sediments and thus the mechanical, hydromechanical and chemical degradation behavior. Therefore, metasediments have been separated according to the metamorphic facies into contact metamorphic (hornfels-sandinite facies: <0.2 GPa, >300°C), intermediate-grade (greenschist-blueschist facies: 0.2–1.2 GPa, 100–450°C), high-grade (amphibolite facies: 0.2–1.2 GPa, 500–750°C), and ultrahigh-grade metamorphic rocks (granulite-eclogite facies). The latter mainly consist of high-grade gneisses and only rarely of granulites (20 measurements). Contact metamorphism includes the transformation of mica schist and gneisses to hornfels and was observed to influence fracture transmissivity [Achtziger-Zupančič *et al.*, 2017; Holland and Witthüser, 2011].

Metaintrusive and metavolcanic rocks are often indistinguishable from their unmetamorphosed lithology, as these rocks experienced similar or higher temperature conditions during emplacement than during subsequent metamorphic overprint. The meta-magmatic rocks are thus compiled in two separate classes. Finally, marbles (calcitic or dolomitic) and brittle homogeneous quartzites are separated into single classes as these rocks presumably constitute extreme hydrogeological environments.

4.2. Local Stress Regime

Differences in the shape of permeability trend curves with depth suggests that gross permeability structure may differ between regions of compressional and extensional tectonic regimes [Achtziger-Zupančič *et al.*, 2017; Manning and Ingebretsen, 1999; Stober and Bucher, 2007; Winkler and Reichl, 2014]. Faulkner and Armitage [2013] underpinned this assumption by testing lab samples of Westerly granite in different stress configurations. In thrust fault regimes (compressional setting) flow is channeled along the intermediate principal stress axis at the margins of the fault zone and is further enhanced by jointing and dilatation in direction of the least principal stress axes [Cox, 2010]. Earnest and Boutt [2014] showed, using a conceptual hydromechanical study in a Toth basin, that depth dependency and spatial variability of hydraulic conductivity are related to deviatoric stress states in depths up to 1000 m.

In our study stress regime determination is based on the world stress map (WSM) database [Heidbach *et al.*, 2008]. Using the closest reasonable stress measurement from the WSM resulted in a wide spectrum of distances up to 800 km. Therefore, upper limits of 10 km and 0.5 km are defined for the horizontal and vertical distances, respectively, to yield more reliable local information (Figure 1). The regimes considered are normal (NF), oblique normal (NS), strike slip (SS), thrust (TF), and oblique thrust faulting (TS). However, only few local stress measurements indicate NF or NS regimes (Table 2 and Figure S7). Most of the nearest stress and hydraulic measurement pairings result from site investigations for geological waste disposal in Northern and Central Europe (Figure 1).

4.3. Seismotectonic Activity

Active tectonics and seismic activity alter the stress field, activate fault slip, and thus create new pathways for groundwater flow [Cox *et al.*, 2014; Ingebretsen and Manning, 2010; Mickelthwaite *et al.*, 2010]. The likely peak ground acceleration (PGA) is a measure of earthquake probability within a certain energy and time frame, which is calculated for rock as reference ground condition (except rock or firm soil in Canada and the U.S.). A worldwide compilation of regional PGA models was accomplished by Giardini *et al.* [1999] and consists of 1° cells covering the entire Earth. The database consists of four hazard classes ranging from low (0–0.8 m/s²) to very high (>4.0 m/s²) accelerations with an exceedance probability of 10% over 50 years. Due to insufficient permeability data, the high (2.4–4.0 m/s²) and very high PGA classes are merged. As numerous permeability data are available in low PGA regions, the low hazard class has been split into very low (0–0.2 m/s²) and low (0.2–0.8 m/s²) PGA classes.

High PGA probabilities are mainly reported from active plate boundaries, resulting in few high to very high PGA values in our database, mainly from Japan, New Zealand, and the west coast of North America (Table 2 and Figure S8). Areas of moderate PGA are mainly situated adjacent to active and passive plate boundaries and also in aborted rifts and occasionally in intraplate situations. Areas of low PGA mainly occur adjacent to moderate PGA zones and in areas with glacial rebound in North America, and in Northern and Central Europe.

4.4. Geological Provinces

Stober and Bucher [2007] and *Ingebritsen and Manning* [2010] suggest that the long-term tectonogeological situation might be an important factor by comparing depth trends of permeability in various geological provinces. *Bucher and Stober* [2010] and *Stotler et al.* [2010] implied the same, comparing the chemical composition of groundwaters. Permeability-depth relationships were also compared by *Ranjram et al.* [2015] for the Fennoscandian Shield (SWE), Southern Germany, and the Molasse Basin (Switzerland); they concluded that tectonic setting exerts controls on shallow permeabilities, but is not important at depths greater than 400 mbgs. In contrast to the local stress regime and PGA, which assess the current tectonic situation, the geological provinces are a proxy for the long-term tectono-geological evolution of a region as they are defined as "any large area or region considered as a whole, all parts of which are characterized by similar features or by a history differing significantly from that of adjacent areas" [Bates and Jackson, 1980]. The tectonogeological setting is denominated according to a modified and extended classification of geological provinces used and applied by the *United States Geological Survey (USGS)* [1997] and described in the Glossary of Geology [Bates and Jackson, 1980].

Most sites in this study are situated in stable positions of shields (i.e., Canadian and Scandinavian Shield) and platforms (i.e., East European Platform). For our analysis we refer to these provinces as "stable provinces." The orogenic provinces are subdivided into active orogens caused by continent-continent collision (e.g., the Alps) or subducting oceanic crusts (e.g., the northern cordilleras), and old, passive orogens, which are still mountain areas but do not show active orogeny (e.g., the Appalachian Mountains, the Black Forest, or the Ore Mountains). Crystalline basement in basins is often covered by several kilometers of sediment; therefore, few basement permeability data exist (Table 2). Nonetheless, our compilation contains sites in fore arc and back arc, foreland and strike-slip basins which are merged for the analysis and referred to as "basin provinces." The distinction between these provinces and the extended crust also included in this compilation, such as rifts and rifted margins, is often subjective. The latter are merged and referred to as "extensional provinces" but still constitute a very small sample number which precludes analysis (Table 2 and Figure S9). We modify the map provided by the *USGS* [1997], splitting Western Europe into several provinces and including both extended crust and passive orogens. Due to the sometimes uncertain delineation of provinces, additional references have been used for some sites in China, West Central Europe, Singapore, and West Central U.S. [e.g., Boulegue et al., 1990; Thury et al., 1994; Wang, 2010; Wang et al., 2006; Zhao et al., 2005].

5. Results

5.1. Global Permeability Trends

Permeabilities from below 2000 mbgs, at or less than the measurement limit, from measurement sections longer than 100 m and from measurement methods with less than 100 individual measurements have been excluded from the analysis, reducing the database from 28,832 permeabilities (cyan dots in Figures 2a and S1) to 19,062 (green dots). The remaining permeabilities range between $1E-22$ and $1E-7\text{ m}^2$. Whenever ranges were reported for single hydraulic tests (i.e., a series of pulse or head/rate tests), the log mean permeabilities are displayed at mean depth (middle of the interval). Otherwise, the individual measurements are shown at mean depth.

The increasing depth increment for permeability averaging with depth (see section 2.3) owes to the decreasing amount of data with depth. While the 0–50 mbgs interval contains over 3000 data points, only 82 individual data are available in the 1500–2000 mbgs interval. Furthermore, while the near-surface data stem from more than 100 regions in 25 countries, the data below 1000 mbgs stem from three to nine regions situated in two to seven countries (mainly in Central Europe). As a result, the permeability distribution below 1000 mbgs depends on a few sites (tunnels, drifts, and galleries in the Aar and Gotthard Massif, Switzerland and the Ore

Mountains, Germany) and may not represent the entire global permeability range. Because the very large data sets from these few sites seem to exhibit a high degree of completeness [Achtziger-Zupančič *et al.*, 2017; Masset and Loew, 2010], the analyses are conducted for the entire depth range to 2000 mbgs. Log mean and log median permeabilities calculated for the depth intervals show that permeability continuously decreases from $1\text{E}{-}14 \text{ m}^2$ at the surface to $1\text{E}{-}17 \text{ m}^2$ at 1500–2000 mbgs (Figures 2a and S1).

A log-log linear fit through all log permeability and log depth pairs results in $\log(k) = -1.5 \times \log(z) - 16.3$ with a RMSE of 1.5 orders of magnitude. The predictive power of this regression ($R^2 = 0.2$) is very low, similar to most of the other regressions discussed later (Table 3). The slope of the regression reveals that the permeability changes average 1.5 orders of magnitude per order of magnitude of depth change. The mean log permeability at 1000 mbgs depth is defined by the intercept as -16.3 m^2 (or $5\text{E}{-}17 \text{ m}^2$). The regression parameters are nearly unaffected by the decreasing amount of data with depth, as seen from similar regression parameters for the data from less than 1000 mbgs and only slightly steeper (-1.7 and -1.8) and shifted (-16.5 and -16.4 m^2) regressions through the mean and median log permeabilities for discrete depth intervals (Table 3).

The range between the maximum and minimum permeabilities decreases with depth, from about 10 orders of magnitude ($1\text{E}{-}19$ to $1\text{E}{-}9 \text{ m}^2$) near the surface to about 7 orders of magnitude in the deepest interval, whereas the 90% and 50% confidence interval are independent of depth at around 5 to 6 orders of magnitude and 1.5 orders of magnitude, respectively. The slope value of the regression through the lower 10% of the permeabilities in each depth interval is substantially lower than the slope value of the regression through the higher 10% of the permeabilities, bordering a larger permeability range with increasing depth and indicating higher data scatter at depth.

The log mean permeability, the log variance, the log skewness, and the resulting metrics of the cluster centroids are shown in gray-scales in Figure 3 as depth profiles of the entire data set and the sub-data sets. The clusters (Figure 3d) are arranged according to increasing log mean permeabilities from black to light grey. Categories with less than three intervals with sufficient data (50 observations, compare Figures S6–S9) are discarded from the grey-scale maps (white areas). The k-means algorithm clusters the sub-data sets according to their similarity in terms of statistical moments (see section 2.4) and results in a three layer hydraulic stratification model (Figure 3d). High mean log permeability around $1\text{E}{-}14 \text{ m}^2$, with high variance of about 2 orders of magnitude, are observed in the uppermost 100 mbgs. To depths of 500 mbgs, the mean log permeability decreases to between $4\text{E}{-}16$ and $1\text{E}{-}15 \text{ m}^2$, with a variance of 2 to 4 orders of magnitude. Below this, permeability further decreases to $3\text{E}{-}17 \text{ m}^2$ with a variance of about 1.7 orders of magnitude. The variance shown in Figure 3b exhibits no significant trend. The skewness increases continuously with depth (Figure 3c), although the skewness is generally not significant [Field, 2000; Trochim and Donnelly, 2001].

5.2. Impact of Technical Factors on Permeability

The categorized sub-data sets for technical factors are shown in the Figures S2 to S5. In Figure 5 and Table 3 the regression parameters (intercept, slope, and RMSE) are shown for the different measurement methods, interval lengths, calculated rock volumes, and orientation categories. Except for open hole tests, the intercepts of the regressions range over a single order of magnitude. The slope values increase in the following order: multipacker tests, open hole hydraulic tests, Lugeon/WD tests, single packer tests, and discrete inflow measurements to tunnels (Figure 5a). The difference flow log method yields a significantly higher slope. The RMSE amounts constantly to about 1 order of magnitude (Figure 5b and Table 3) except for packer tests (around 1.5 order of magnitude).

The regressions through the three sub-data sets defined by orientation exhibit very similar slopes and intercepts. The RMSE increases slightly with verticality from 1.0 to 1.6 orders of magnitude, although observations are also more abundant (Figure 5 and Tables 2 and 3).

The longer the measurement section, the steeper the slopes and the lower the intercept (Figure 5a and Table 3). The RMSE and the predictive power (R^2) increase slightly with interval length (Figure 5b and Table 3). The means of the calculated rock test volumes increase slightly with depth, independent of the measurement method (Figure 4). Distinct means and ranges of calculated rock test volumes can be allocated to the different measurement methods. The volume range of multipacker tests encompass those of the other

test methods, except for the discrete inflow measurements into tunnels. We conduct the analysis of test volumes separately for tunnel inflows in order to investigate scaling effects (Figure S4). Regressions are calculated for each order of magnitude increment in test volume between $1E-3$ to $1E6\text{ m}^3$ and $1E4$ to $1E8\text{ m}^3$ for borehole and tunnel-based tests, respectively (Table 3). The slope values of the borehole-based regressions generally flatten from -2 to -1 as the intercepts increase from $1E-19$ to $1E-13\text{ m}^2$ with increasing test volume (Figure 5a). The RMSE increases with size of each sub-data set (compare Tables 2 and 3). A similar trend of increasing intercepts is observed for increasing test volumes of tunnel inflow-based values, but with a shift of 3 to 4 orders of magnitude toward lower permeabilities in comparison to borehole-based tests (Figure 5a). The slope and RMSE values are relatively constant but higher for the tunnel inflow-based permeabilities.

5.3. Impact of Geological Factors on Permeability

The categorized sub-data sets for all geological factors are shown in Figures S6 through S9. In Figure 6, illustrative sub-data sets are shown. Geological province and seismic activity are the most influential factors, as inferred from the distribution of regression parameters for geological factors with sufficient permeability data, shown in Figure 7 and Table 3. The slopes of the regressions range between -1.2 (high to very high PGA) and -2.4 (marble), and the intercepts from $5E-16$ (high to very high PGA) to $8E-18\text{ m}^2$ (passive orogens). The regression intercepts (permeability at 1000 mbgs), shown in Figure 7a, increase nearly linearly with decreasing steepness of the log-log regressions. The steep slopes imply relatively high permeabilities close to the surface and very low permeabilities deeper underground. As seen by the R^2 values (Table 3: 0.01 to 0.55), most regressions exhibit low predictive power, whereas the RMSE is in a narrow band of 1 to 2 orders of magnitude (Figure 7b and Table 3). As shown in Figure 3, the mean, variance, and skewness of log permeability decrease with depth for most geological factors. However, the observed trend is strongly scattered for skewness and weak for variance.

5.3.1. Lithology

In general, all the magmatic and high- to ultrahigh-grade metamorphic rocks exhibit about similar depth trends, independent of mineralogical composition and whether the rocks experienced metamorphism or not. The RMSE spans about 1.5 orders of magnitude for metamorphic intrusives and increases with decreasing SiO_2 content to more than 2 orders of magnitude for basic and ultrabasic rocks (Figure 7 and Table 3). The grey scale maps (Figure 3) indicate that intermediate and basic intrusives generally exhibit slightly higher mean log permeability and higher variance compared to the acidic intrusives.

The steepness of slope decreases from contact to intermediate-grade metamorphic rocks, high- and ultrahigh-grade metamorphic rocks (Figure 7a and Table 3). Mean log permeability of contact and intermediate metamorphic rocks are similarly low below 700 mbgs and is higher for contact metamorphic rocks above 300 mbgs (Figure 3a). In accordance with the grey scale map of the variance (Figure 3b) the RMSE increases with the grade of regional metamorphism but is highest for contact metamorphic rocks (Figure 7b and Table 3).

The regression through the permeabilities tested in marble exhibits the lowest intercept and the lowest slope value (Figure 7) and a low RMSE (0.8 times). Quartzites show permeabilities which follow the same slope as the general regression, but the intercept is higher by 0.75 orders of magnitude (Figure 7a and Table 3).

5.3.2. Local Stress Regimes

Due to the low number of observations, normal fault (NF) and oblique normal fault regimes (NS) have not been included, and analysis of the strike slip regimes (SS) have been limited to the uppermost 600 mbgs (Table 2), excluding the depth trend (Figure S7). The grey scale map of mean log permeability exhibits higher permeabilities for the uppermost 300 mbgs and 500–600 mbgs for SS (Figure 3a) in comparison to thrust fault (TF) and oblique thrust fault regimes (TS), also showing higher mean log permeability, log variances, and log skew at any depth for TS in comparison to TF which results in high-permeability clusters for TS below 300 mbgs (Figure 3). The intercepts of the regressions fairly agree but the slope through the TS data is steeper than for TF (Figure 7a and Table 3). Both data sets exhibit about the same size and data scatter as seen from RMSE (Figure 3b and Tables 2 and 3).

5.3.3. Seismotectonic Activity (PGA)

Regions with high PGA exhibit the highest slope value, the highest intercept, and highest RMSE (Figure 7a and Table 3), corresponding to high mean log permeability and log variances in depth intervals with

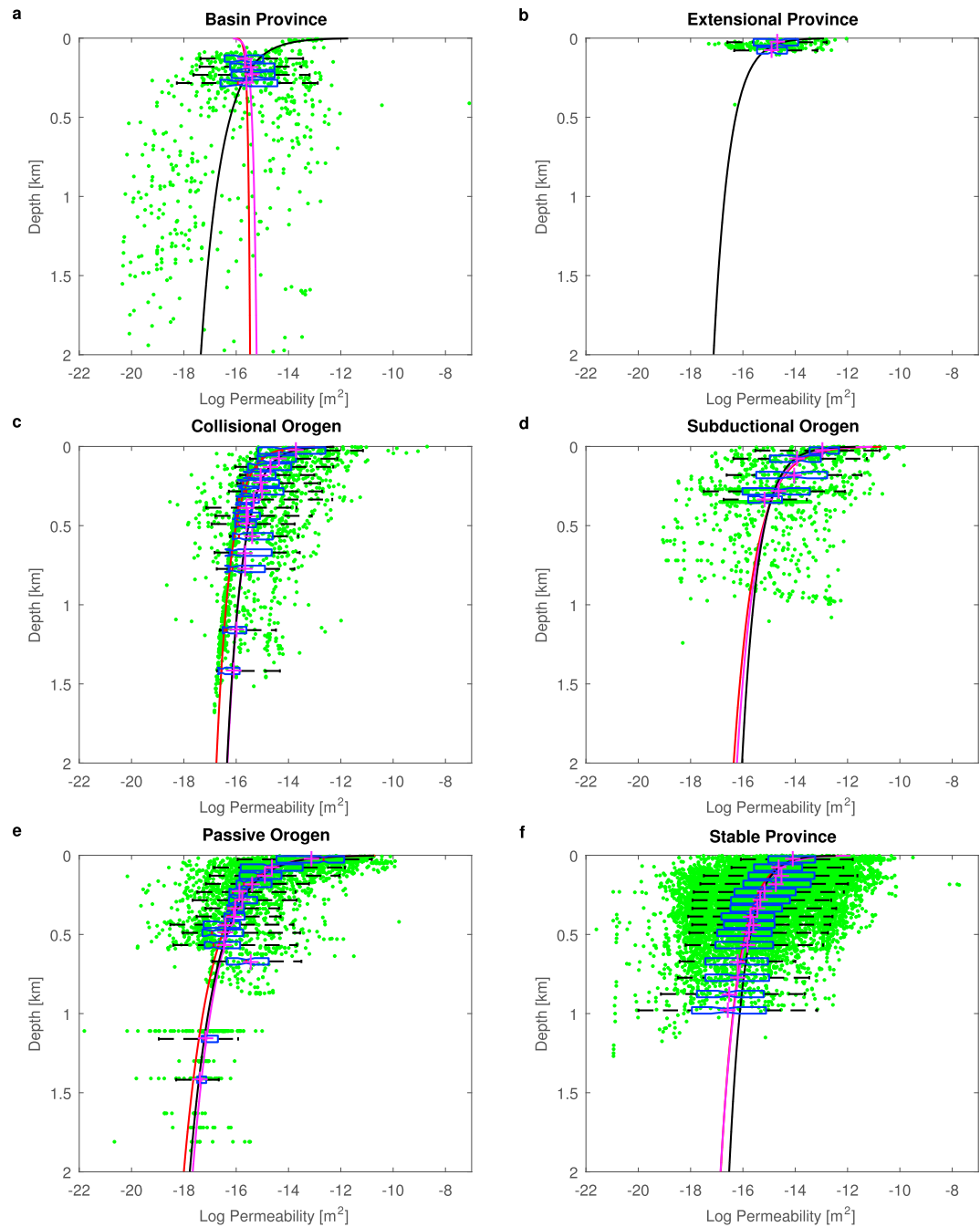


Figure 6. Illustrative sub-data sets showing the depth trend of permeability (green) and its regression (black, solid line), the mean log k (pink crosses) and the median log k (red center of the boxplot) with 50% (blue) and 90% (black, dashed line) confidence interval at each depth for the geological provinces. The red and the pink solid curves describe the regression through the log median and the log mean permeability, respectively. For comparison the depth range is fixed to 2 km intentionally, although some data sets are restricted to shallower depth.

sufficient data (Figures 3a and 3b). With the exception of very low PGA regions, there is a general trend toward a lower slope value and lower intercept as PGA decreases (Figure 7a and Table 3). These dependencies are also reflected in the cluster analysis, where the high-permeability clusters in highly active regions extend to 300 mbgs depth, and the lowest permeability cluster is observed at comparably shallow depths of 500 mbgs in regions with very low PGA (Figures 3a and 3d).

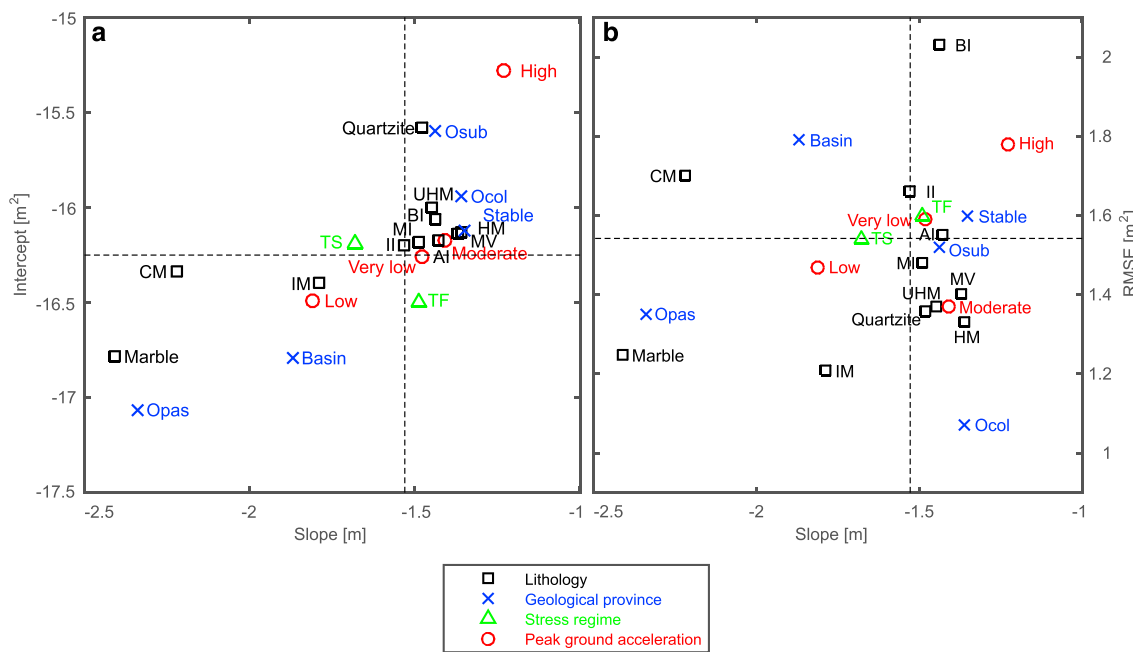


Figure 7. Parameters of regression through the permeability measurements for sub-data sets defined by geological factors. CM, contact metamorphic; IM, intermediate-grade metamorphic; HM, high-grade metamorphic; UHM, ultrahigh-grade metamorphic; MV, metavolcanic; MI, metaintrusive; AI, acidic intrusive; II, intermediate intrusive; BI, basic intrusive; Opas, passive orogen; Ocol, continent-continent collisional orogen; Osub, subduction related orogen; TF, thrust fault regime; TS, oblique thrust fault regime. The intersection of the dashed lines shows where the regression parameters of the entire data set plot. (a) Intercept versus the slope of the regression. (b) Root-mean-square error (RMSE) versus the slope of the regression.

5.3.4. Geological Province

As seen from the greyscale maps in Figure 3, stable provinces (Stable) exhibit a consistent decrease of permeability and a trend toward increasing variance with depth (Figures 3a and 3b). The skewness is constant around zero (Figure 3c). Clear differences are seen in the orogenic provinces. The active provinces (Ocol and Osub) exhibit generally higher mean log permeability and skewness and systematically lower variances than the stable provinces for all analyzable depths, while passive orogens (Opas) tend to have the lowest mean log permeabilities and intermediate variances (Figures 3a–3c). This is reflected by the similar slope value of stable provinces and active orogens, higher than in basin provinces (Basin) and passive orogens (Figure 7a and Table 3). The intercept is highest for subduction (Osub) related orogens and generally decreases with increasing steepness of slope.

6. Discussion

6.1. Uncertainties and Limitations of the Global Permeability Data Set

Using legacy and published data has one important drawback: permeability data are collected with a purpose, and therefore there may be a sampling bias at individual sites [see also Scibek *et al.*, 2016]. We tried to overcome this problem by using a wealth of globally distributed data acquired for different purposes (e.g., water supply, site characterization for dams and nuclear waste disposal, mining, tunneling, and geothermal energy). Measurement intervals longer than 100 m and permeabilities at the measurement limit of a method are discarded, changing the permeability-depth relations for some sites—e.g., Black Forest [Stober and Bucher, 2007], Hästhömen/Finland [Pöllänen and Rouhiainen, 1998a, 1998b], and Ore Mountains/Germany [Achtziger-Zupančič *et al.*, 2017]. Thus, the permeability distribution is truncated at the lower end, resulting in higher mean log permeabilities and a shift of regression curves toward higher permeabilities. The derived permeability trends indicate probably an upper limit of mean values. The uncertainty of the multiregression analysis is low, as each sub-data set is treated separately. The decreasing amount of data with depth is also considered a minor problem, because similar regression parameters are calculated for mean/median log permeability and the measurements for maximum depths of 1000 mbgs and 2000 mbgs (Table 3). Major differences are attributed to regression through only few

single measurements or few mean/median log permeabilities (e.g., marble, quartzite, and strike-slip regime), a factor mitigated by requiring a minimum number of observations.

6.2. Decrease of Permeability and Specific Storage With Depth

Crystalline rocks are generally low-conductivity media, where secondary porosity from fractures dictates hydraulic behavior at borehole and site scale [e.g., *Long et al.*, 1996; *Rutqvist and Stephansson*, 2003]. The connected pore space provided by fracturing imprints a highly heterogeneous flow field at site scale. However, the permeability-depth relationships are directionally independent, indicating that preferential sampling and permeability anisotropy are not major concerns (Figure 5). This is unexpected, as the orientation of permeable fractures often changes from moderately inclined in the upper 200 to 300 mbgs to steeply inclined at greater depths [*Boult et al.*, 2010; *Follin and Stigsson*, 2014; *Masset and Loew*, 2013; *Mattila and Tammisto*, 2012; *Mazurek*, 1998].

Still, the scatter of test scale permeability is high at any given depth, and permeabilities should be described as a range over a particular depth interval [*Ingebritsen and Manning*, 2010; *Stober and Bucher*, 2007], resulting in a low predictive power for a single regression curve. The observed range of permeabilities in each depth interval is constant at around 1.5 and 5 orders of magnitude for the 50 and 90% confidence intervals, respectively, possibly reflecting the strong variations of permeability around brittle fault zones [*Achtziger-Zupančič et al.*, 2016]. The decreasing frequency of extremely high permeabilities with depth likely results from reduced apertures of larger fractures due to increased stresses at depth [e.g., see *Rutqvist and Stephansson*, 2003].

That mean permeability decreases by 3 to 4 orders of magnitude in the upper 2000 mbgs of the crust has been observed at many sites around the globe [e.g., *Masset and Loew*, 2010; *Ranjam et al.*, 2015; *Shmonov et al.*, 2003; *Stober and Bucher*, 2007]. Higher permeabilities close to the surface are the result of near-surficial stress relaxation and chemomechanical alteration [*Henriksen*, 1995; *Lachassagne et al.*, 2011; *Pan et al.*, 1995]. At greater depths, the water flow is controlled by partially mineralized fractures [*Rutqvist and Stephansson*, 2003]. Fracture normal stiffness is stress magnitude dependent [e.g., *Zangerl et al.*, 2008]. In consequence, the permeable fracture spacing increases nonlinearly with depth as seen at many sites, for instance, in the Ore Mountains [*Achtziger-Zupančič et al.*, 2017], and the rock mass permeability decreases. Below about 1000 mbgs, the primary, lithology-dependent matrix porosity exerts increasing control with depth and becomes the defining factor for rock mass permeability. The resulting trend for the entire data set yields a similar intercept but a slightly lower slope value than the “generalized k versus z equation” of *Stober and Bucher* [2007]. In agreement with these authors, the slope at shallow depths in the Earth’s crust (0–2 km) is significantly less steep and the interception is lower than the widely used “standard curve” derived by *Manning and Ingebritsen* [1999].

Permeability and specific yield/storage exhibit surprisingly similar depth trends, with the slope at 1000 mbgs being -1.5 for the permeability trend and -1.0 for specific storage/yield. The high storage values of around $1E-4 \text{ m}^{-1}$ in the upper 200 mbgs represent the behavior of a phreatic aquifer in fractured rocks with a drainable porosity of about 0.01%. In the same depth interval we observe a very large scatter with values as low as $3E-8 \text{ m}^{-1}$ indicating local occurrence confined fracture flow already in the upper few 100 mbgs. The transition from unconfined to confined fracture flow seems to be gradual and does not occur at a clear depth level. The correspondence in slope of permeability and specific storage at 1000 m depth cannot be explained easily, but at greater depth both specific storage and permeability are influenced by matrix porosity.

6.3. Scale Effects

The calculated test volumes are similar for all borehole tests but significantly smaller than the rock test volumes calculated for tunnel-based measurements (Figure 4). A comparison of permeability ranges from these two types of tests shows overall similarities, although the distribution of permeabilities from the tunnel-based measurements is more skewed toward lower values. The slopes for similar tested rock volumes are similar, but the intercept is 3 to 4 orders of magnitude lower for the tunnel-based measurements (compare classes between $1E4$ and $1E6 \text{ m}^3$ in Figure 5). That difference may result from fracture closure around draining and open tunnels at great depth (HM coupling), non-Darcy-type flow in rough-walled fractures close to the excavation or degassing effects [*Fernandez and Moon*, 2010; *Mas Ivars*, 2006; *Masset and Loew*, 2013]. However, the detailed mechanisms responsible for these differences in calculated scale effects are unknown.

A scale effect can be inferred from the decreasing intercept and steepening of slope with increasing test interval length. Single and multipacker tests were mostly conducted over the shortest intervals. Intermediate intervals are characteristic of difference flow logs and multipacker tests. The longest intervals consist of samples from discrete inflow measurements to tunnels (1/3) and other measurement methods (2/3). Permeability increase with increasing rock test volume is observed, affecting both the slope and intercept. However, this is not an independent finding, as the calculated radii of influence, and thus the calculated test volumes, are dependent on the permeability itself. The observed scale effect might also be influenced by permeability and specific yield/storage being treated as uncorrelated in the derivation of test volumes. Nevertheless, 1 order of magnitude change in the calculated test volume causes a change of 0.6 orders of magnitude of permeability, which is close to the factor of 0.55 observed by *Illman and Tartakovsky* [2006] from cross-hole hydraulic tests performed at the Grimsel Test Site (Switzerland).

6.4. Geological Provinces and Seismotectonic Activity as Main Factors Controlling the Permeability Distribution

As shown by the multiple regression (Figure 7) and cluster analyses (Figure 3), the tectonogeological history (expressed as geological province) and the current seismotectonic activity (expressed as PGA) exert the main control on site scale permeabilities in the upper 2 km of the crystalline crust. Intercept and slope of the regressions are correlated for both of these geological factors.

The Global Seismic Hazard Map GSHAP used in this study results from historical and instrumental seismic catalogs, earthquake source and ground-shaking models, and depicts Peak Ground Acceleration (PGA) for a recurrence period of 475 years. It is well known that permeability increases in fault zones after seismic events, when preferential flow paths are enhanced or newly created [Cox *et al.*, 2014; Kitagawa *et al.*, 2007; Wang and Manga, 2010]. Within a few years or decades, permeability progressively returns to the preseismic conditions due to mineralization of the fractures [Brenguier *et al.*, 2008; Kelly *et al.*, 2013]. The available data set is rich for all PGA classes down to at least 1000 m depth (Figure S8).

The higher slope value in high-PGA regions may result from steeply dipping and interconnected faults which act as preferential conduits for flow [Kitagawa *et al.*, 2007; Shi and Wang, 2016]. The general decrease of permeability with decreasing seismic activity indicates that fracturing or shearing are the dominating processes controlling permeability for all geological provinces and lithologies considered. The intermediate permeabilities encountered in regions with very low seismic hazard are mainly derived from sites situated on continental shields subjected to postglacial rebound (Canada, Finland, and Sweden). This suggests that other factors like aseismic fault creep triggered by postglacial rebound (indicated by recent uplift or subsidence rates) may be important.

Major control on permeability is also exerted by the long-term tectonogeological history for which the geological province serves as a proxy (Figures 3 and 7). The difference between active and inactive orogens is striking. In many active orogens, including those caused by both continent-continent collision and subduction of oceanic crust, preferentially vertical faults and fractures are reactivated older structures. Associated igneous intrusion causes hydraulic fracturing orthogonal to the surface of the intrusion in its hot state and surface parallel jointing in its cooling phase. Furthermore, topography alters the stress field to a depth of 2 or 3 times the elevation difference (in young orogens potentially a few kilometers) [Pan *et al.*, 1995]. As a result, a dense network of young, partially mineralized open fractures and faults is imprinted, providing the necessary secondary porosity for flow controlled by steep hydraulic gradients caused by the topography. We suggest that these processes result in the observed high permeability and higher slope. Higher permeabilities of subduction-related orogens, in comparison to continent-continent collisional orogens, might be caused by high seismotectonic activity in the circum-Pacific Ring of Fire, in contrast to low to intermediate seismic activity of many collisional orogens (e.g., the Alps).

Due to their long deformation history, passive orogens are usually intensely fractured and faulted. In contrast to the active orogens, the fractures are often healed and sealed, mineralized, or filled with fine-grained cataclastic material and weathering products, as observed, for example, in the Ore Mountains [Achtziger-Zupančič *et al.*, 2017, 2016]. The fracture infill may be locally weathered and washed out, resulting in higher permeabilities close to the surface and a steep permeability gradient. Creation or reactivation of faults and fractures is rare, as these regions usually exhibit low to very low tectonic and seismic activity. Stable

provinces were expected to constitute a low-permeability environment, but with a higher slope value as the topography is shallow. However, as this province is mainly found in Canada and Scandinavia, the relatively high intercept may result from reactivation of structures caused by glacial rebound.

Crystalline basement rocks in basins show significantly increased permeability, which may result from older preserved fracture networks and paleosurfaces below a thick sedimentary cover, as observed, for example, in deep exploration boreholes in the Molasse basin of Northern Switzerland [Thury *et al.*, 1994, and references therein]. Additionally, basins are usually created by normal faults and extensional tectonics that increase permeability [Faulkner and Armitage, 2013].

6.5. Lithology

In our global database, lithology exerts only minor control on the permeability distribution. High- and ultrahigh-grade metamorphic, metavolcanic, metaintrusive, and intrusive rocks have seen similar stress-temperature paths, and thus similar mechanical properties have been imprinted. This global result is in contradiction to single sites where lithologic control on hydraulic properties has been observed [e.g., Gustafson and Krásný, 1994; Masset and Loew, 2010; Stober, 1995], probably resulting from differing rock textures and accompanying mechanical anisotropies [Hoek and Martin, 2014; Masset and Loew, 2010; Stober, 1995]. A steeper slope for intermediate-grade metamorphic rocks may result from low subsurface permeabilities resulting from higher rock compressibility [Hoek and Diederichs, 2006], intensified by a higher amount of potentially swelling and water-retaining phyllosilicates [Achtziger-Zupančič *et al.*, 2017; Davies and Ó Dochartaigh, 2002], and higher permeabilities at the surface, which may indicate greater sensitivity to weathering and alteration.

Some specialized rock types show major differences. Contact metamorphic rocks are intensively fractured through hydrothermal fracturing, increased brittleness, metasomatism, and cooling induced jointing [Driesner, 2010; Ingebritsen *et al.*, 2010] and exhibit a distinct brittleness contrast relative to the granite and the unaltered rock mass. Especially around young intrusions, permeability is enhanced [Matter *et al.*, 2005] and remnants may persist over Mio of years [Achtziger-Zupančič *et al.*, 2017; Baudoin and Gay, 1996; Holland and Witthüser, 2011]. Marbles exhibit a steep slope due to high surficial permeabilities, probably resulting from (paleo) karst, and low permeabilities deeper underground, where dissolution of the otherwise low-porosity rock is minimal. A shift toward higher permeabilities for quartzites may reflect very brittle behavior. For these latter two rock classes, the analysis is more uncertain, as relatively few observations are available.

In general, the influence of rock composition may be underestimated here, as often all lithologies discovered at a single site, borehole, or drift section are assigned to all permeabilities tested there.

6.6. A New Prediction Algorithm of Permeability Distribution at Site Scale

The fitting parameters given in Table 3 have been validated using leave-one-out cross validation for the entire data set. The permeability value of each measurement is assumed unknown, then predicted based on the regression relationships. The prediction error is analyzed as a metric of the model accuracy, the RMSE of the predictions being used as an indicator of the performance of the regression relationships. On average the RMSEs of the leave-one-out cross validation are well within the RMSE of the model regression, indicating the applicability and the high predictive power of the regression equations.

The predictive power of the derived regression coefficients has been tested on two independent permeability data sets from Austria and Guyana. The first permeability data set has been derived from packer tests conducted in boreholes drilled through a deep-seated rockslide adjacent to the Gepatsch reservoir (Klasingarten, Austria) [Strauhal *et al.*, 2016]. The available in situ permeability measurements are separated into measurements conducted in the sliding rock mass (blue dots in Figure 8a) and measurements conducted in the stable crystalline basement (red dots). The undisturbed rock mass below the rockslide consists of amphibolite facies para-gneisses (high-grade metamorphic rocks) with quartzite intercalations (quartzite), which were assumed to be equally distributed. The eastern Alps are a continent-continent collisional orogen with PGA values in the range of 0.8 to 1.3 m/s² (moderate hazard). The average regression curve (consisting from 1/6 of the regression parameters of both lithologic units, 1/3 of the geological province and 1/3 of the PGA class) predicts $\log(k) = -1.4 \times \log(z) - 16.0$ with an error band of about 1.3 orders of magnitude (Figure 8a). A weighting of the single factors was not performed as this could be interpreted as a tuning parameter.

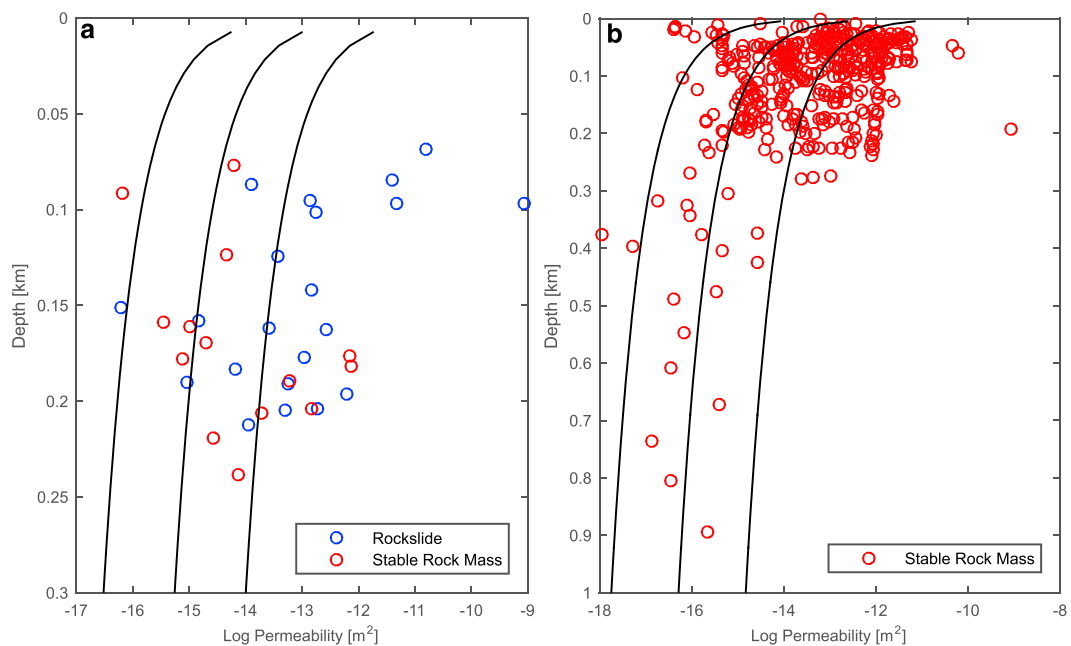


Figure 8. Predicted permeability distribution for (a) the Klasgarten rockslide site (bounds represent the predicted RMSE or standard deviation). The blue and red dots show permeability measurements conducted in the sliding mass and in the stable rock mass, respectively. (b) Permeability prediction and measurements at the Aurora Gold Project in Guyana (bounds represent the predicted RMSE or standard deviation).

When considering the depth trend of measured permeabilities in stable bedrock, we observe an excellent correspondence with our model prediction, including the RMSE.

The same validation procedure has been applied to a second independent test case, consisting of more than 400 individual hydraulic packer and open borehole tests collected for a feasibility study at the Aurora Gold Project (Guyana) to a depth of about 900 mbgs. The rock mass mainly consists of greenschist facies metamorphosed sediments and metavolcanic rocks, which are assumed to be equally distributed. The site is situated on the Guyana Shield, a low-PGA region ($0.4\text{--}0.8 \text{ m/s}^2$). The averaged prediction regression results in $\log(k) = -1.6 \times \log(z) - 16.3$ with an error band of about 1.5 orders of magnitude. The results displayed in Figure 8b show that the permeability-depth relationships for the stable basement rocks are again correctly predicted. The predicted range is shifted toward lower values in the upper 250 mbgs at the Aurora site, probably resulting from most hydraulic tests being performed in metavolcanic dikes which are well connected to the nearby river. The RMSE values at both sites almost correspond to the model confidence intervals, with a slight underestimation of 0.2 orders of magnitude.

7. Summary and Conclusions

In this study, a comprehensive global database of hydrogeological properties of crystalline basement rocks has been compiled and evaluated by means of multivariate statistics. The database consists of about 29,000 permeability measurements from 221 publications and unpublished data from 30 countries. The database is derived from in situ borehole and tunnel hydraulic and tracer tests, hypocenter movements, or calibrated groundwater flow models. After applying quality control, 19,062 measurements remained for statistical analyses which reflect the hydraulic behavior of crystalline basement rocks into depths of 2000 mbgs.

Hydraulic measurements in boreholes and drifts are purpose driven and therefore highlight distinct ranges of permeability and tested rock volume. A scale dependency of permeability is observed on calculated test volumes, equal to 0.6 orders of magnitude of permeability change per order of magnitude of rock volume change. However, only a few in situ data are available for independent validation. The orientation of the measurement or sampling line, and therefore preferential sampling and hydraulic anisotropy, are of negligible importance.

Regression analyses performed on the entire permeability data set exhibit a clear depth dependence by $\log(k) = -1.5 \times \log(z) - 16.3$ or more than 3 orders of magnitude to 2000 mbgs depth, indicating that increasing depth (and stress) is a primary control on permeability. However, the scatter of data is high, with a 90% confidence interval ranging across 5 orders of magnitude independent of depth. This scatter is strongly influenced by permeability variations around brittle fault zones. A k-means clustering was performed based on log mean, log variance, and log skewness of the entire permeability data set and sub-data sets separated by depth interval and geological factors. The clustering results in a three-layer hydraulic model consisting of a surficial high-permeability zone, a zone of flow dominated by partially mineralized fractures, and a zone of matrix-controlled flow. Specific yield and storage values exhibit a similar slope as the general permeability trend, as seen from a compilation of about 30 independently measured specific yield and specific storage ranges over the same depth interval. While in the upper 200 mbgs fracture flow varies between confined and unconfined, we only observe confined fracture and matrix flow below about 600 m depth.

Current seismotectonic activity, with peak ground acceleration (PGA) as a proxy, and the long-term tectono-geological history, with geological province as a proxy, are the most important geological factors controlling the permeability distribution. The steepness of the regressions increases and the permeability intercept at 1000 mbgs depth decreases with decreasing PGA. Also, a clear difference is observed between active orogens, exhibiting a higher slope value and a high-permeability intercept, and inactive orogens, with a low slope value and low-permeability intercept. The regression parameters for basin provinces and stable provinces fall in between. Generally, lithology has minor impact, with the exception of specialized rock types such as marble, contact metamorphic rocks (both steep slope and low intercept) and quartzites (flat slope and high intercept), which probably result from mechanical properties and chemical resistance of these rocks. However, the differences between all analyzed geological factors is not more than 2 orders of magnitude with 1 to 2 orders of standard error at any given depth.

Type curves are derived for the geological factors and validated by leave-one-out cross validation. These model curves are successfully tested on two independent data sets.

Appendix A

The dynamic viscosity of pure water was approximated by equation (A1):

$$\mu(Ta) = 2.414 \times 10^{-5} \times 10^{247.8/Ta-140} \quad (A1)$$

where μ is the dynamic viscosity of water in kg/(m s) and Ta is the (estimated) absolute temperature in °K. Equation (A1) is valid in the temperature range 0 to 370°C and predicts the dynamic viscosity of pure water with an accuracy of 2.5% [Al-Shemmeri, 2012].

The density of water in kg/m³ has been estimated using equation (A2) [Kuder, 2011, and references therein]:

$$\rho_{\text{Fluid}} = \rho^{\text{Ta}} + \Delta\rho^P + 1000 \times \text{TDS} \quad (A2)$$

with

$$\rho^T = \frac{a_0 + a_1 \times \text{Ta} + a_2 \times \text{Ta}^2 + a_3 \times \text{Ta}^3 + a_4 \times \text{Ta}^4 + a_5 \times \text{Ta}^5}{(1 + b \times \text{Ta})} \quad (A3)$$

with $a_0 = 999,84$; $a_1 = 16,95$; $a_2 = -7,99E-3$; $a_3 = -4,62E-5$; $a_4 = 1,06E-7$; $a_5 = -2,81E-10$ and $b = 0,017$ and

$$\Delta\rho^P = p \times 4.0625 \times 10^{-7} \quad (A4)$$

where ρ^T is the density of water at Ta, $\Delta\rho^P$ is the change in density for a given hydrostatic pressure change. The pressure p in Pa is assumed to be hydrostatic and thus only dependent on the saturated overburden. The influence of the content of total dissolved solids (TDS) has been neglected as it is seldom reported and nearly no depth gradients are available [Ranjam et al., 2015; Stober and Bucher, 2007].

Acknowledgments

We thank, especially, J. Scibek (McGill) for the cooperation during the painful search and compilation of data and discussion of ideas. For the scientific support, enriching discussions, and the provision of data, we thank Ph. Blum (KIT), B. Lanyon (Fracture Systems Ltd.), D. Faulkner (U. Liverpool), Th. Driesner, J.A.D. Connolly, and former and current members of the Engineering Geology group at ETHZ. Additionally, we thank Steven Ingebritsen, Tom Gleeson and the Editors for careful improvements and corrections. The authors declare no conflict of interest. The data for this paper and all related references are stored at the crustal permeability data repository (<http://crustalpermeability.weebly.com/data-sources.html>).

References

- Achtziger-Zupančič, P., S. Loew, A. Hiller, and G. Mariethoz (2016), 3D fluid flow in fault zones of crystalline basement rocks (Poehla-Tellerhaeuser Ore Field, Ore Mountains, Germany), *Geofluids*, 16(4), 688–710, doi:10.1111/gfl.12192.
- Achtziger-Zupančič, P., S. Loew, and A. Hiller (2017), Factors controlling the permeability distribution in fault vein zones surrounding granitic intrusions (Ore Mountains/Germany), *J. Geophys. Res. Solid Earth*, 122, 1876–1899, doi:10.1002/2016JB013619.
- Ahokas, H., J. Pöllänen, P. Rouhiainen, and A. Kuusela-Lahtinen (2013), Quality review of transmissivity data from Olkiluoto site—Drillholes OL-KR1-KR57 WR-2012-99, 392 pp., Posiva OY, Helsinki.
- Al-Shemmeri, T. (2012), *Engineering Fluid Mechanics*, p. 140, Bookboon.com, Staffordshire.
- Almén, K.-E., J.-E. Andersson, L. Carlsson, K. Hansson, and N.-A. Larsson (1986), Hydraulic testing in crystalline rock, in *A Comparative Study of Single-Hole Test Methods*, 179 pp., SKB, Stockholm.
- Arthur, D., and S. Vassilvitskii (2007), K-means++: The advantages of careful seeding, in *Proceedings of the Eighteenth Annual ACM-SIAM Symposium on Discrete Algorithms*, edited, pp. 1027–1035, Soc. for Ind. and Appl. Math., New Orleans, La.
- Balla, Z., and P. Molnár (2004), General characteristics of the Bátaapáti (Üveghuta) site (South-western Hungary), *Annu. Rep. Geol. Inst. Hungary*, 2003, 73–91.
- Bates, R. L., and J. A. Jackson (1980), *Glossary of Geology*, p. 749, Am. Geol. Inst., Falls Church, Va.
- Baudoin, P., and D. Gay (1996), Stockage direct – étude comparative du risque radiologique des stockages de combustibles usés et de déchets vitrifiés en formation géologique profonde de type granitique 279, 165 pp., Institut de Protection de Surete Nucléaire.
- Bense, V. F., T. Gleeson, S. E. Loveless, O. Bour, and J. Scibek (2013), Fault zone hydrogeology, *Earth Sci. Rev.*, 127, 171–192, doi:10.1016/j.earscirev.2013.09.008.
- Berkowitz, B. (2002), Characterizing flow and transport in fractured geological media: A review, *Adv. Water Resour.*, 25(8–12), 861–884, doi:10.1016/S0309-1708(02)00042-8.
- Black, J. H., D. C. Holmes, and M. Brightman (1987), *Crosshole Investigations—Hydrogeological Results and Interpretations NTB 87-37*, p. 77, Nagra, Baden.
- Boulegue, J., M. Benedetti, B. Gauthier, and B. Bosch (1990), Les fluides dans le socle du sondage GPF Sancerre-Couy, *Bull. Soc. Géol. Fr.*, VI(5), 789–795, doi:10.2113/gssgbull.VI.5.789.
- Boutt, D. F., P. Diggins, and S. Mabee (2010), A field study (Massachusetts, USA) of the factors controlling the depth of groundwater flow systems in crystalline fractured-rock terrain, *Hydrogeol. J.*, 18(8), 1839–1854, doi:10.1007/s10040-010-0640-y.
- Brace, W. F. (1978), Note on permeability changes in geologic material due to stress, *Pure Appl. Geophys.*, 116(4–5), 627–633, doi:10.1007/bf00876529.
- Brace, W. F. (1980), Permeability of crystalline and argillaceous rocks, *Int. J. Rock Mech. Min. Sci.*, 17(5), 241–251, doi:10.1016/0148-9062(80)90807-4.
- Bredehoeft, J. D., and S. S. Papadopoulos (1980), A method for determining the hydraulic properties of tight formations, *Water Resour. Res.*, 16, 233–238, doi:10.1029/WR016i001p00233.
- Brenguier, F., M. Campillo, C. Hadzioannou, N. M. Shapiro, R. M. Nadeau, and E. Larose (2008), Postseismic Relaxation Along the San Andreas Fault at Parkfield from Continuous Seismological Observations, *Science*, 321(5895), 1478–1481, doi:10.1126/science.1160943.
- Bucher, K., and I. Stober (2010), Fluids in the upper continental crust, *Geofluids*, 10(1–2), 241–253, doi:10.1111/j.1468-8123.2010.00279.x.
- Butler, J. J., and J. M. Healey (1998), Relationship between pumping-test and slug-test parameters: Scale effect or artifact?, *Ground Water*, 36(2), 305–312, doi:10.1111/j.1745-6584.1998.tb01096.x.
- Carlsson, L., and T. Olson (1985), Hydrogeological and hydrogeochemical investigations in boreholes: Final report, *Stripa Project TR 85-10*, 107 pp., SKB, Stockholm.
- Clauer, C. (1991), Permeabilität kristalliner Gesteine—Vergleich von Mittelwerten im Massstab 0.01 bis 10000 Metern, 21 pp., Niedersächsisches Landesamt für Bodenforschung, Hannover.
- Clauer, C. (1992), Permeability of crystalline rocks, *Eos*, *Trans. AGU*, 73(21), 233–238, doi:10.1029/91EO00190.
- Cooper, H. H., J. D. Bredehoeft, and S. S. Papadopoulos (1967), Response of a finite-diameter well to an instantaneous charge of water, *Water Resour. Res.*, 3, 263–269, doi:10.1029/WR003i001p00263.
- Cox, S. C., C. D. Menzies, R. Sutherland, P. H. Denys, C. Chamberlain, and D. A. H. Teagle (2014), Changes in hot spring temperature and hydrogeology of the alpine fault hanging wall, New Zealand, induced by distal South Island earthquakes, *Geofluids*, doi:10.1111/gfl.12093.
- Cox, S. F. (2010), The application of failure mode diagrams for exploring the roles of fluid pressure and stress states in controlling styles of fracture-controlled permeability enhancement in faults and shear zones, *Geofluids*, 10(1–2), 217–233, doi:10.1111/j.1468-8123.2010.00281.x.
- Davies, J., and B. E. Ó Dochartaigh (2002), Low permeability rocks in sub-Saharan Africa: Groundwater development in the Tabora region, Tanzania CR/02/191N, 66 pp., Nottingham.
- Davis, S. N., and L. J. Turk (1964), Optimum depth of wells in crystalline rocks, *Ground Water*, 2(2), 6–11, doi:10.1111/j.1745-6584.1964.tb01750.x.
- Delisle, G. (1975), Determination of permeability of granitic rocks in GT-2 from hydraulic fracturing data LA-6169-MS United States 10.2172/7200324 Thu Mar 24 09:15:23 EDT 2011 Dep. NTIS LANL; ERA-01-08412 English, Medium: P; Size: Pages: 5 pp.
- Denzel, S., T. Behnert, T. Ertel, R. Dinkel, and U. Trost (1997), Handbuch Altlasten und Grundwasserschadensfälle-Methodensammlung, 176 pp., Planungsgemeinschaft Umweltwirtschaft GmbH und Weber-Ingenieure, Karlsruhe.
- Driesner, T. (2010), The interplay of permeability and fluid properties as a first order control of heat transport, venting temperatures and venting salinities at mid-ocean ridge hydrothermal systems, *Geofluids*, 10(1–2), 132–141, doi:10.1111/j.1468-8123.2009.00273.x.
- Earnest, E., and D. Boutt (2014), Investigating the role of hydromechanical coupling on flow and transport in shallow fractured-rock aquifers, *Hydrogeol. J.*, 22(7), 1573–1591, doi:10.1007/s10040-014-1148-7.
- Faulkner, D. R., and P. J. Armitage (2013), The effect of tectonic environment on permeability development around faults and in the brittle crust, *Earth Planet. Sci. Lett.*, 375, 71–77, doi:10.1016/j.epsl.2013.05.006.
- Fernandez, G., and J. Moon (2010), Excavation-induced hydraulic conductivity reduction around a tunnel—Part 1: Guideline for estimate of ground water inflow rate, *Tunnelling Underground Space Technol.*, 25(5), 560–566, doi:10.1016/j.tust.2010.03.006.
- Field, A. (2000), *Discovering Statistics Using SPSS for Windows*, Edited, Sage Publ., London-Thousand Oaks-New Delhi.
- Follin, S., and M. Stigsson (2014), A transmissivity model for deformation zones in fractured crystalline rock and its possible correlation to in situ stress at the proposed high-level nuclear waste repository site at Forsmark, Sweden, *Hydrogeol. J.*, 22(2), 299–311, doi:10.1007/s10040-013-1078-9.

- Frape, S. K., and P. Fritz (1987), Geochemical trends for groundwaters from the Canadian shield, in *Saline Water and Gases in Crystalline Rocks*, vol. 33, edited by P. Fritz and S. K. Frape, pp. 19–38, Geol. Assoc. of Can. Spec. Pap., The Runge Press Limited, Ottawa.
- Freeze, R. A., and J. A. Cherry (1979), *Groundwater*, p. 604, Prentice Hall, Englewood Cliffs, N. J.
- Gale, J. E. (1982), Assessing the permeability characteristics of fractured rock, *Geol. Soc. Am., Spec. Pap.;(United States)*, 189(CONF-790284-), 163–182.
- Gascoyne, M., C. C. Davison, J. D. Ross, and R. Pearson (1987), Saline groundwaters and brines in plutons in the Canadian shield, *Saline Water Gases Cryst. Rocks*, 33, 53–68.
- Giardini, D., G. Grunthal, K. M. Shedlock, and P. Z. Zhang (1999), The GSHAP global seismic hazard map, *Ann. Geofis.*, 42(6), 1225–1230.
- Gleeson, T., L. Smith, N. Moosdorf, J. Hartmann, H. H. Dürr, A. H. Manning, L. P. H. van Beek, and A. M. Jellinek (2011), Mapping permeability over the surface of the Earth, *Geophys. Res. Lett.*, 38, L02401, doi:10.1029/2010GL045565.
- Gleeson, T., N. Moosdorf, J. Hartmann, and L. P. H. van Beek (2014), A glimpse beneath Earth's surface: Global Hydrogeology MaPS (GLHYMPS) of permeability and porosity, *Geophys. Res. Lett.*, 41, 3891–3898, doi:10.1002/2014GL059856.
- Guéguen, Y., P. Gavrilenko, and M. Le Ravalec (1996), Scales of rock permeability, *Surv. Geophys.*, 17(3), 245–263, doi:10.1007/BF01904043.
- Gustafson, G., and J. Krásný (1994), Crystalline rock aquifers: Their occurrence, use and importance, *Appl. Hydrogeol.*, 2(2), 64–75, doi:10.1007/s100400050051.
- Heidbach, O., M. Tingay, A. Barth, J. Reinecker, D. Kurfeß, and B. Müller (2008), The world stress map database release., edited, Potsdam/Heidelberg, doi:10.1594/GFZ.WSM.Rel2008.
- Heitfeld, M., P. Mohrdieck, and K. Schetelig (1998), Eignung verschiedener Durchlässigkeitsversuche, in *Geotechnik Hydrogeologie*, pp. 495–508, Springer, Berlin, Heidelberg, doi:10.1007/978-3-642-58851-8_11.
- Henriksen, H. (1995), Relation between topography and well yield in boreholes in crystalline rocks, *Sogn og Fjordane, Norway, Ground Water*, 33(4), 635–643, doi:10.1111/j.1745-6584.1995.tb00319.x.
- Henriksen, H. (2008), Late quaternary regional geodynamics and hydraulic properties of the crystalline rocks of Fennoscandia, *J. Geodyn.*, 45(1), 49–62, doi:10.1016/j.jog.2007.05.001.
- Hoek, E., and M. S. Diederichs (2006), Empirical estimation of rock mass modulus, *Int. J. Rock Mech. Min. Sci.*, 43(2), 203–215, doi:10.1016/j.ijrmms.2005.06.005.
- Hoek, E., and C. D. Martin (2014), Fracture initiation and propagation in intact rock—A review, *J. Rock Mech. Geotech. Eng.*, 6(4), 287–300, doi:10.1016/j.jrmge.2014.06.001.
- Holland, M., and K. T. Withhüser (2011), Evaluation of geologic and geomorphologic influences on borehole productivity in crystalline bedrock aquifers of Limpopo Province, South Africa, *Hydrogeol. J.*, 19(5), 1065–1083, doi:10.1007/s10040-011-0730-5.
- Horne, R. N. (1995), *Modern Well Test Analysis—A Computer-Aided Approach*, Petroway Inc, Palo Alto, Ca.
- Illman, W. A., and D. M. Tartakovsky (2006), Asymptotic analysis of cross-hole hydraulic tests in fractured granite, *Ground Water*, 44(4), 555–563, doi:10.1111/j.1745-6584.2006.00201.x.
- Illman, W. A., X. Liu, S. Takeuchi, T.-C. J. Yeh, K. Ando, and H. Saegusa (2009), Hydraulic tomography in fractured granite: Mizunami underground research site, Japan, *Water Resour. Res.*, 45, W01406, doi:10.1029/2007WR006715.
- Ingebretsen, S. E., and T. Gleeson (2015), Crustal permeability: Introduction to the special issue, *Geofluids*, 15(1/2), 1–10, doi:10.1111/gfl.12118.
- Ingebretsen, S. E., and C. E. Manning (1999), Geological implications of a permeability-depth curve for the continental crust, *Geology*, 27(12), 1107–1110, doi:10.1130/0091-7613(1999)027<1107:GIOAPD>2.3.CO;2.
- Ingebretsen, S. E., and C. E. Manning (2003), Implications of crustal permeability for fluid movement between terrestrial fluid reservoirs, *J. Geochem. Explor.*, 78–79, 1–6, doi:10.1016/S0375-6742(03)00037-2.
- Ingebretsen, S. E., and C. E. Manning (2010), Permeability of the continental crust: Dynamic variations inferred from seismicity and metamorphism, *Geofluids*, 10(1–2), 193–205, doi:10.1111/j.1468-8123.2010.00278.x.
- Ingebretsen, S. E., S. Geiger, S. Hurwitz, and T. Driesner (2010), Numerical simulation of magmatic hydrothermal systems, *Rev. Geophys.*, 48, RG1002, doi:10.1029/2009RG000287.
- Ishii, E. (2015), Predictions of the highest potential transmissivity of fractures in fault zones from rock rheology: Preliminary results, *J. Geophys. Res. Solid Earth*, 120, 2220–2241, doi:10.1002/2014JB011756.
- Jacob, C. E., and S. W. Lohman (1952), Nonsteady flow to a well of constant drawdown in an extensive aquifer, *Trans. Am. Geophys. Union*, 33, 559–569.
- Jiang, X.-W., X.-S. Wang, and L. Wan (2010), Semi-empirical equations for the systematic decrease in permeability with depth in porous and fractured media, *Hydrogeol. J.*, 18(4), 839–850, doi:10.1007/s10040-010-0575-3.
- Japan Nuclear Cycle Development Institute (JNC) (2000), H12: Project to establish the scientific and technical basis for HLW disposal in Japan — Supporting report 1: Geological environment in Japan, TN 1410-2000-002, 352 pp., Jpn. Nucl. Cycle Dev. Inst. (JNC), Tokai, Ibaraki.
- Kaufman, L., and P. J. Rousseeuw (1990), *Finding Groups in Data: An Introduction to Cluster Analysis*, 342 pp., John Wiley, Hoboken N. J., doi:10.1002/9780470316801.
- Kelly, C. M., A. Rietbrock, D. R. Faulkner, and R. M. Nadeau (2013), Temporal changes in attenuation associated with the 2004 M6.0 Parkfield earthquake, *J. Geophys. Res. Solid Earth*, 118, 630–645, doi:10.1002/jgrb.50088.
- Kitagawa, Y., K. Fujimori, and N. Koizumi (2007), Temporal change in permeability of the Nojima fault zone by repeated water injection experiments, *Tectonophysics*, 443(3–4), 183–192, doi:10.1016/j.tecto.2007.01.012.
- Kruseman, G. P., and N. A. de Ridder (1991), *Analysis and Evaluation of Pumping Test Data*, ILRI, Wageningen, Netherlands.
- Kuder, J. (2011), Methoden zur Berechnung von Fluidparametern, 0129716, 26 pp., Leibniz-Institut für Angewandte Geophysik Hannover, Hannover.
- Kwak, H. T., G. Zhang, and S. Chen (2005), The effects of salt type and salinity on formation water viscosity and NMR responses, paper presented at proceedings of the international symposium of the Society of Core Analysts, Toronto, Canada.
- Lachassagne, P., R. Wyns, and B. Dewandel (2011), The fracture permeability of hard rock aquifers is due neither to tectonics, nor to unloading, but to weathering processes, *Terra Nova*, 23(3), 145–161, doi:10.1111/j.1365-3121.2011.00998.x.
- Lawson, D. W. (1968), Groundwater flow systems in the crystalline rocks of the Okanagan Highland, British Columbia, *Can. J. Earth Sci.*, 5(4), 813–824, doi:10.1139/e68-079.
- Lee, P. K., R. Pearson, R. E. J. Leech, and R. Dickin (1982), Hydraulic testing of deep fractures in the Canadian shield, *Bull. Int. Assoc. Eng. Geol.*, 26–27(1), 461–465, doi:10.1007/BF02594259.
- Leech, R. E. J., K. G. Kennedy, and D. Gevaert (1984), *Sondierbohrung Böttstein—Hydrogeologic Testing of Crystalline Rocks*, p. 155, Nagra, Baden.
- Lloyd, S. P. (1982), Least squares quantization in PCM, *IEEE Trans. Inf. Theory*, 28(2), 129–137, doi:10.1109/TIT.1982.1056489.
- Lomize, G. M. (1951), Flow in fractured rocks, *Gosenergoizdat*, Moscow, 127.

- Long, J. C. S., et al. (1996), *Rock Fractures and Fluid Flow: Contemporary Understanding and Applications*, Natl. Acad. Press, Washington, D. C.
- Ludvigson, J.-E., K. Hansson, and P. Rouhiainen (2002), Methodology study of Posiva difference flow meter in borehole KLX02 at Laxemar, 87 pp., Svensk Kärnbränslehantering AB, Stockholm.
- Manga, M., I. Beresnev, E. E. Brodsky, J. E. Elkhouri, D. Elsworth, S. E. Ingebritsen, D. C. Mays, and C.-Y. Wang (2012), Changes in permeability caused by transient stresses: Field observations, experiments, and mechanisms, *Rev. Geophys.*, 50, RG2004, doi:10.1029/2011RG000382.
- Manning, C. E., and S. E. Ingebritsen (1999), Permeability of the continental crust: Implications of geothermal data and metamorphic systems, *Rev. Geophys.*, 37, 127–150.
- Maréchal, J. C., B. Dewandel, and K. Subrahmanyam (2004), Use of hydraulic tests at different scales to characterize fracture network properties in the weathered-fractured layer of a hard rock aquifer, *Water Resour. Res.*, 40, W11508, doi:10.1029/2004WR003137.
- Mas Ivars, D. (2006), Water inflow into excavations in fractured rock—A three-dimensional hydro-mechanical numerical study, *Int. J. Rock Mech. Min. Sci.*, 43(5), 705–725, doi:10.1016/j.ijrmms.2005.11.009.
- Masset, O., and S. Loew (2010), Hydraulic conductivity distribution in crystalline rocks, derived from inflows to tunnels and galleries in the Central Alps, Switzerland, *Hydrogeol. J.*, 18(4), 863–891, doi:10.1007/s10040-009-0569-1.
- Masset, O., and S. Loew (2013), Quantitative hydraulic analysis of pre-drillings and inflows to the Gotthard Base tunnel (Sedrun lot, Switzerland), *Eng. Geol.*, 164, 50–66, doi:10.1016/j.enggeo.2013.06.002.
- Mather, J. D., and F. P. Sargent (1986), Determination of the characteristics of crystalline rocks by field experiments: A review, *Philos. Trans. R. Soc. Lond. Series A, Math. Phys. Sci.*, 319(1545), 139–156, doi:10.1098/rsta.1986.0091.
- Matter, J. M., D. S. Goldberg, R. H. Morin, and M. Stute (2005), Contact zone permeability at intrusion boundaries: New results from hydraulic testing and geophysical logging in the Newark Rift Basin, New York, USA, *Hydrogeol. J.*, 14(5), 689–699, doi:10.1007/s10040-005-0456-3.
- Mattila, J., and E. Tammisto (2012), Stress-controlled fluid flow in fractures at the site of a potential nuclear waste repository, Finland, *Geology*, 40(4), 299–302, doi:10.1130/g32832.1.
- Mazurek, M. (1998), Geology of the crystalline basement of northern Switzerland and derivation of geological input data for safety assessment models 1015–2636, Nagra, Wettingen.
- Mazurek, M. (2000), Geological and hydraulic properties of water-conducting features in crystalline rocks, in *Hydrogeology of Crystalline Rocks*, edited by I. Stober and K. Bucher, pp. 3–26, Springer, Dordrecht.
- McEwen, T., and T. Äikäs (2000), The site selection process for a spent fuel repository in Finland, *Summary Rep. 9516521010*, 224 pp., Posiva OY, Helsinki.
- Micklethwaite, S., H. A. Sheldon, and T. Baker (2010), Active fault and shear processes and their implications for mineral deposit formation and discovery, *J. Struct. Geol.*, 32(2), 151–165, doi:10.1016/j.jsg.2009.10.009.
- Nastev, M., M. M. Savard, P. Lapcevic, R. Lefebvre, and R. Martel (2004), Hydraulic properties and scale effects investigation in regional rock aquifers, south-western Quebec, Canada, *Hydrogeol. J.*, 12(3), 257–269, doi:10.1007/s10040-004-0340-6.
- Paillet, F. L., J. H. Williams, J. Urik, J. Lukes, M. Kobr, and S. Mares (2012), Cross-borehole flow analysis to characterize fracture connections in the Melechov granite, Bohemian-Moravian Highland, Czech Republic, *Hydrogeol. J.*, 20(1), 143–154, doi:10.1007/s10040-011-0787-1.
- Pan, E., B. Amadei, and W. Z. Savage (1995), Gravitational and tectonic stresses in anisotropic rock with irregular topography, *Int. J. Rock Mech. Min. Sci. Geomech. Abstr.*, 32(3), 201–214, doi:10.1016/0148-9062(94)00046-6.
- Pöllänen, J., and P. Rouhiainen (1998a), Difference flow measurements at the Hästholmen site in Loviisa, boreholes KR1-KR3, WR-97-41e, 165 pp., Posiva OY, Helsinki.
- Pöllänen, J., and P. Rouhiainen (1998b), Difference flow measurements at the Hästholmen site in Loviisa, boreholes KR4-KR6 and Y8 WR-1998-28, 176 pp., Posiva OY, Helsinki.
- Prinz, H., and R. Strauß (2012), *Ingenieurgeologie*, 5th ed., p. 737, Springer, Heidelberg.
- Ranjram, M., T. Gleeson, and E. Luijendijk (2015), Is the permeability of crystalline rock in the shallow crust related to depth, lithology or tectonic setting?, *Geofluids*, 15(1/2), 106–119, doi:10.1111/gfl.12098.
- Rawling, G. C., P. Baud, and T.-F. Wong (2002), Dilatancy, brittle strength, and anisotropy of foliated rocks: Experimental deformation and micromechanical modeling, *J. Geophys. Res.*, 107(B10), 2234, doi:10.1029/2001JB000472.
- Rumble, D. (1994), Water circulation in metamorphism, *J. Geophys. Res.*, 99, 15499–15502, doi:10.1029/94JB01148.
- Rutqvist, J. (2015), Fractured rock stress-permeability relationships from in situ data and effects of temperature and chemical-mechanical couplings, *Geofluids*, 15(1/2), 48–66, doi:10.1111/gfl.12089.
- Rutqvist, J., and O. Stephansson (2003), The role of hydromechanical coupling in fractured rock engineering, *Hydrogeol. J.*, 11(1), 7–40, doi:10.1007/s10040-002-0241-5.
- Schulze-Makuch, D., D. A. Carlson, D. S. Cherkauer, and P. Malik (1999), Scale dependency of hydraulic conductivity in heterogeneous media, *Ground Water*, 37(6), 904–919, doi:10.1111/j.1745-6584.1999.tb01190.x.
- Schulze-Makuch, D., and D. S. Cherkauer (1998), Variations in hydraulic conductivity with scale of measurement during aquifer tests in heterogeneous, porous carbonate rocks, *Hydrogeol. J.*, 6(2), 204–215, doi:10.1007/s10040050145.
- Scibek, J., T. Gleeson, and J. M. McKenzie (2016), The biases and trends in fault zone hydrogeology conceptual models: Global compilation and categorical data analysis, *Geofluids*, doi:10.1111/gfl.12188.
- Shapiro, A. M., J. A. Ladderd, and R. M. Yager (2015), Interpretation of hydraulic conductivity in a fractured-rock aquifer over increasingly larger length dimensions, *Hydrogeol. J.*, 23(7), 1319–1339, doi:10.1007/s10040-015-1285-7.
- Shi, Z., and G. Wang (2016), Aquifers switched from confined to semiconfined by earthquakes, *Geophys. Res. Lett.*, 43, 11,166–111,172, doi:10.1002/2016GL070937.
- Shmonov, V. M., V. M. Vitovtova, A. V. Zharikov, and A. A. Grafchikov (2003), Permeability of the continental crust: Implications of experimental data, *J. Geochem. Explor.*, 78–79, 697–699, doi:10.1016/S0375-6742(03)00129-8.
- Sievänen, U. (2001), Leakage and groutability, *WR-2001-06*, 86 pp., Posiva OY, Helsinki.
- Snow, D. T. (1968), Hydraulic character of fractured metamorphic rocks of the front range and implications to the Rocky Mountain arsenal well, *Colo. School Mines Q.*, 63(1), 167–199.
- Snow, D. T. (1979), *Packer Injection Test Data from Sites on Fractured Rock*, p. 15, LBNL, Springfield, Va.
- Steiner, W., A. Thut, H. Fisch, and H.-J. Gysi (2006), Geohydraulische Versuche in Fels VSS 2001/505, 82 pp., B+S Ingenieure AG, Solexperts AG, Gysi Leoni Mader AG, Bern.
- Stevenson, D. R., E. T. Kozak, C. C. Davison, M. Gascoyne, and R. A. Broadfoot (1996), Hydrogeologic characteristics of domains of sparsely fractured rock in the granitic Lac du Bonnet batholith, southeastern Manitoba, Canada, Atomic Energy of Canada Ltd., Whiteshell Labs., Pinawa, MB, Canada.
- Stober, I. (1995), *Die Wasserführung des kristallinen Grundgebirges*, p. 191, Enke, Stuttgart.

- Stober, I. (1997), Permeabilities and chemical properties of water in crystalline rocks of the Black Forest, Germany, *Aquat. Geochem.*, 3(1), 43–60, doi:10.1023/A:1009623432059.
- Stober, I., and K. Bucher (2007), Hydraulic properties of the crystalline basement, *Hydrogeol. J.*, 15(2), 213–224.
- Stober, I., and K. Bucher (2015), Hydraulic conductivity of fractured upper crust: Insights from hydraulic tests in boreholes and fluid-rock interaction in crystalline basement rocks, *Geofluids*, 15(1–2), 161–178, doi:10.1111/gfl.12104.
- Stotler, R. L., S. K. Frape, and O. Shouakar-Stash (2010), An isotopic survey of $\delta^{81}\text{Br}$ and $\delta^{37}\text{Cl}$ of dissolved halides in the Canadian and Fennoscandian shields, *Chem. Geol.*, 274(1–2), 38–55, doi:10.1016/j.chemgeo.2010.03.014.
- Strahal, T., S. Loew, M. Holzmann, and C. Zangerl (2016), Detailed hydrogeological analysis of a deep-seated rockslide at the Gepatsch reservoir (Klasgarten, Austria), *Hydrogeol. J.*, 24(2), 349–371, doi:10.1007/s10040-015-1341-3.
- Thury, M., A. Gautschi, M. Mazurek, W. H. Müller, H. Naef, F. J. Pearson, S. Vomvoris, and W. Wilson (1994), Geology and hydrogeology of the crystalline basement of northern Switzerland: Synthesis of regional investigations 1981–1993 within the Nagra Radioactive Waste Disposal Programme., *Tech. Rep. NTB 93–01*, 449 pp., Natl. Coop. for Disposal of Radioactive Waste (NAGRA), Wettingen.
- Trochim, W. M. K., and J. P. Donnelly (2001), *Research Methods Knowledge Base*, Atomic Dog, Cincinnati, Ohio.
- United States Geological Survey (USGS) (1997), *Geologic Province and Thermo-Tectonic Age Maps*, U.S. Geol. Surv., Menlo Park, Calif.
- Vovk, I. F. (1987), Radiolytic salt enrichment and brines in the crystalline basement of the east European Platform, in *Saline Water and Gases in Crystalline Rocks*, edited by P. Fritz and S. Frape, *Geol. Assoc. Can. Spec. Pap.*, 33, 197–210.
- Wang, C.-Y., and M. Manga (2010), Hydrologic responses to earthquakes and a general metric, *Geofluids*, 10(1–2), 206–216, doi:10.1111/j.1468-8123.2009.00270.x.
- Wang, J. (2010), High-level radioactive waste disposal in China: Update 2010, *J. Rock Mech. Geotech. Eng.*, 2(1), 1–11.
- Wang, J., R. Su, W. Chen, Y. Guo, Y. Jin, Z. Wen, and Y. Liu (2006), Deep geological disposal of high-level radioactive wastes in China, *Chin. J. Rock Mech. Eng.*, 4, 000.
- West, F. G., P. R. Kintzinger, and W. D. Purtymun (1975), Hydrologic testing geothermal test hole no. 2 LA-6017-MS United States10.2172/5083607Thu Mar 24 08:59:34 EDT 2011Dep. NTISLANLEnglish, Medium: ED; Size: Pages: 8 pp.
- Winkler, G., and P. Reichl (2014), Scale dependent hydraulic investigations of faulted crystalline rocks—Examples from the Eastern Alps, Austria, *Fract. Rock Hydrogeol.*, 20, 181–196.
- Wong, T.-F., and W. Zhu (2013), Brittle faulting and permeability evolution: Hydromechanical measurement, microstructural observation, and network modeling, in *Faults and Subsurface Fluid Flow in the Shallow Crust*, edited by W. C. Haneberg, pp. 83–99, AGU, Washington, D. C., doi:10.1029/GM113p0083.
- Zangerl, C., K. F. Evans, E. Eberhardt, and S. Loew (2008), Technical note, *Int. J. Rock Mech. Min. Sci.*, 45(8), 1500–1507, doi:10.1016/j.ijrmms.2008.02.001.
- Zeithöfer, M., B. Wagner, and T. Spörlein (2015), Strukturgeologie und Grundwasserführung im ostbayrischen Grundgebirge, 64 pp., Bayrischen Landesamt für Umwelt, Augsburg.
- Zha, Y., T.-C. J. Yeh, W. A. Illman, T. Tanaka, P. Bruines, H. Onoe, and H. Saegusa (2015), What does hydraulic tomography tell us about fractured geological media? A field study and synthetic experiments, *J. Hydrol.*, 531(Part 1), 17–30, doi:10.1016/j.jhydrol.2015.06.013.
- Zhao, J., A. M. Hefny, and Y. X. Zhou (2005), Hydrofracturing in situ stress measurements in Singapore granite, *Int. J. Rock Mech. Min. Sci.*, 42(4), 577–583, doi:10.1016/j.ijrmms.2005.02.002.
- Zimmermann, G., H. Burkhardt, and L. Engelhard (2003), Scale dependence of hydraulic and structural parameters in the crystalline rock of the KTB, *Pure Appl. Geophys.*, 160(5), 1067–1085, doi:10.1007/pl00012561.
- Zlotnik, V. A., B. R. Zurbuchen, T. Ptak, and G. Teutsch (2000), Support volume and scale effect in hydraulic conductivity: Experimental aspects, *Geol. Soc. Am. Spec. Pap.*, 348, 215–231, doi:10.1130/0-8137-2348-5.215.